UNIVERSITATEA BABEŞ-BOLYAI
BABEŞ-BOLYAI TUDOMÁNYEGYETEM
BABEŞ-BOLYAI UNIVERSITÄT
BABEŞ-BOLYAI UNIVERSITY
TRADITIO ET EXCELLENTIA

BABEŞ-BOLYAI UNIVERSITY
Faculty of Chemistry and Chemical Engineering

Summary

Artificial Neural Networks Based Modelling and Optimization for Improving the Wastewater Treatment Plant Operation

PhD Candidate: Eng. Mihály Norbert-Botond
Supervisor: Prof. PhD Eng. Vasile Mircea Cristea

Cluj-Napoca, 2024

Summary table of contents

Thesis table of contents

Keywords

wastewater treatment plant; artificial neural network modelling; greenhouse gas emissions; effluent quality; energy consumption; genetic algorithms; plant operation optimization; fault detection and identification.

1. Introduction

1.1. Motivation and background

Greenhouse gases (GHGs) are necessary for life to exist on earth as they produce the greenhouse effect, which helps the planet retain the heat from the sun and causing the surface to naturally warm, however, when the GHG concentrations rise excessively additional heat gets trapped leading to the increase of global temperature [1].

The three main anthropogenic GHGs are carbon dioxide (CO_2), methane (CH_4), and nitrous oxide (N_2O) with varying contribution levels towards global warming. The atmospheric concentrations of GHGs have reached all-time highs in 2019 for CO_2 (410 ppm), CH_4 (1866 ppb), as well as N_2O (332 ppb) as depicted in Figure 1.1. These have contributed to an increase in global surface temperature of about 1.1 °C compared to values in 1850-1900 [2].

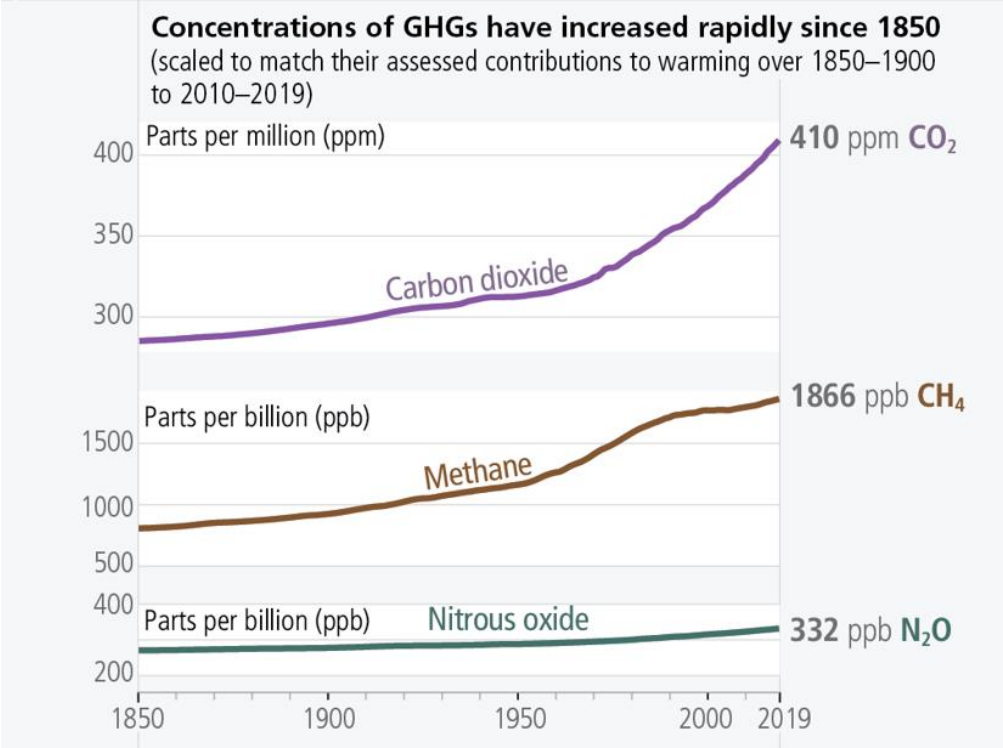

Figure 1.1 Increase of GHG concentrations in the atmosphere [2]

It is also important to take note of the GHG emission sources and activities that contribute to emissions on a global scale, coupled with the type of gases related to each activity, presented in Figure 1.6 for 2019.

The energy sector accounts for almost 76% of total emissions with electricity and heat production as the largest share of 31.8%. The International Energy Agency (IEA) [3] determined that in 2019, despite a 1.3% decrease in CO2 emissions from power production, the power sector was still the main source of these emissions, accounting for 41% of all energy-related CO_2 emissions [4].

Wastewater emissions encompass all of the major GHGs as the accumulation of organic matter and residuals from plants, animals, humans, and the waste produced by them decomposes resulting in emissions of carbon dioxide, methane, as well as nitrous oxide [5,6]. Wastewater is attributed 1.3% of global GHG emissions and around 1% of the worldwide energy consumption. As a consequence, there has been an increase in popularity in the study of their energy consumption and GHG emissions.

Municipal wastewater treatment has frequently been carried out in an unsustainable manner, with significant energy demands, resulting in a substantial impact on climate change. The quantity and quality of influent wastewater as well as the treatment method have a significant impact on the WWTPs energy demand [7]. The quantity of global wastewater production is undergoing a constant growth due to the growth of the human population and the quickening pace of industrialization [8], and is expected to reach an increase of 51% by 2050 in comparison with current levels [9]. At the same time, the increasingly stricter regulations regarding effluent quality led to the development and application of more advanced treatment technologies, however, these also increased the plant's energy demand [10]. As the majority of the energy originates form non-renewable sources, more than 70% of the worldwide energy production in 2022, its generation is accompanied by significant emissions [11].

The research of WWTP control technologies in view of GHG emission reduction gains significance considering international agreements, especially in the case of urban plants that encounter steadily growing flow rate of influent while striving to meet GHG reduction goals. Lowering energy demand and GHG emissions in WWTPs may be accomplished by optimizing energy efficiency in terms of structure and equipment, energy recovery processes, technical procedures, and cost management. It is clear that adopting a more energy-efficient strategy may reduce both operational costs and energy demand [12].

1.2. Models commonly used in the WWTP field of study

Activated sludge process modelling is now often used in the design and operation of WWTPs. It is necessary to take numerous factors into consideration when simulating the activated sludge systems, which encompasses processes like carbon oxidation, nitrification and denitrification. The first aim was to develop a model with minimum of complexity, which resulted in the Activated Sludge Model No. 1, also known as ASM1. When the knowledge on the underlying processes of the biological phosphorus removal grew, the Task Group integrated both the biological nitrogen removal and biological phosphorus removal into a new

model, the Activated Sludge Model No. 2 (ASM2). The ASM2 model was expanded to the Activated Sludge Model No. 2d (ASM2d) with the inclusion of denitrifying PAOs. The most recent modelling platform, the Activated sludge Model No. 3, was developed with the potential of tracking internal storage compounds, that are crucial to organisms' metabolisms [13].

1.2.1. Activated Sludge Model No. 1

The Task Group embraced the idea of switching functions to toggle the process rate equations on and off as the environmental conditions are modified. This was especially important for processes that were reliant on the sort of available electron acceptor, as biological processes depend on heterotrophic or autotrophic bacteria. This phenomenon can be described by incorporating a dissolved oxygen switch into the process rate equations, as presented in Eq. (1.1).

$$\frac{S_O}{K_O+S_O} \tag{1.1}$$

where S_O represents the dissolved oxygen level.

In this manner, by assigning a relatively smaller value to *Ko* the switching function's value is close to unity for moderate dissolved oxygen (DO) concentrations but drops to zero as the DO concentration reaches zero. A similar approach can be adopted for processes that require the absence of dissolved oxygen through a switching function in the form shown in Eq. (1.2).

$$\frac{K_O}{K_O+S_O} \tag{1.2}$$

Another important aspect of the model is that the organic matter present in wastewater was subdivided into a number of categories, as well as the fact that both the mass balances and concentrations were based on chemical oxygen demand (COD) units. This unit was selected from the three measures commonly utilized, i.e., biological oxygen demand (BOD), total organic carbon, and COD, as it was considered to offer a connection not only between the biomass and oxygen consumption, but also to the electron equivalents in the substrate.

The very first distinction between types of organic matter can be made based on their biodegradability. A non-biodegradable material passes through unaltered when entering an activated sludge system due to it being biologically inert. Further subdivision can be made taking into account the physical state of the matter, which can be soluble or particulate. The inert soluble matter is noted as S_I and its concentration in the effluent remains unchanged compared to the influent concentration. The suspended counterpart, X_I, is eliminated from the system as sludge waste after being entangled in the activated sludge. Similarly, biodegradable organic matter can also be divided into readily biodegradable and slowly biodegradable

parts. In order to ease the modelling process, the readily biodegradable part, noted as S_S, is considered soluble, while the slowly biodegradable matter (X_S) is taken as particulate.

Heterotrophic biomass ($X_{B,H}$) is produced in either anoxic or aerobic circumstances by growth on the readily biodegradable substrate and is considered to halt under anaerobic conditions. Loss of biomass due to decay is also incorporated in the model taking into account death, predation, lysis, and endogenous metabolism. This process is considered to result in slowly biodegradable substrate and other particulate matter, X_P, that do not take part in further biological processes.

Similar to carbonaceous matter, nitrogenous matter in wastewater may also be broken down into two categories: non-biodegradable and biodegradable, each with further subcategories. The particulate part of the non-biodegradable nitrogen compounds is linked to the non-biodegradable particulate COD, while the soluble category was chosen not be detailed in the model due to its minor amount. In terms of the biodegradable nitrogenous matter, this can be further divided into: ammonia (S_{NH}), i.e., the free compound as well as its salts; soluble organic nitrogen, noted as S_{ND}; and particulate organic nitrogen, X_{ND}. Heterotrophic bacteria interact with the soluble organic nitrogen and transform it into ammonia nitrogen. Ammonia nitrogen is then used as an energy source for autotrophic nitrifying bacteria as well as a source of nitrogen for the synthesis of heterotrophic biomass. For the sake of simplicity, it is assumed that the autotrophic conversion of ammonia nitrogen to nitrate nitrogen is a one-step process that demands oxygen. Figure 1.3 illustrates, the complex interactions of the system components modelled as 8 processes in the ASM1.

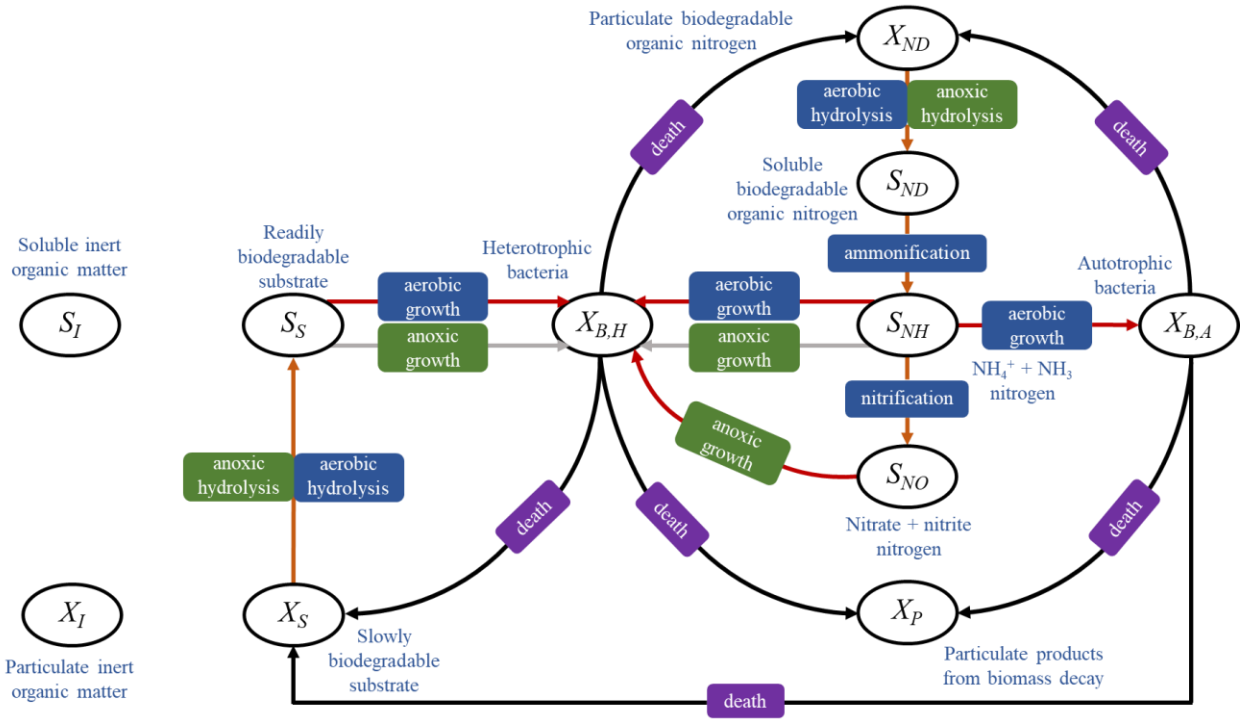

Figure 1.2 General scheme of the ASM1

1.2.2. Activated Sludge Model No. 2d

To take into consideration the notion that phosphorus accumulating organisms (PAOs) may utilise cell-internal organic storage products for denitrification, two more processes were introduced. ASM2d features denitrifying PAOs, in contrast to ASM2 which limited the growth of PAOs to only aerobic circumstances.

ASM2 includes poly-phosphates, a portion of the activated sludge that is crucial for the operation of the activated sludge system but does not exert any COD, in contrast to ASM1, which was based solely on COD for all particulate organic material and the total concentration of the activated sludge. This leads to the potential for total suspended solids (TSS) inclusion in the model. Additionally, TSS permits the incorporation of mineral particulate solids in the influent to treatment facilities as well as the creation of such particles in the context of phosphorus precipitation.

Compared to the 8 processes that were taken into account for the development of ASM1, the ASM2d incorporates a total of 21 processes, which are briefly described below.

The hydrolysis reactions do, in fact, depend on the electron acceptor present, and as such three processes were differentiated in order to fully describe the hydrolysis process:

1. Aerobic hydrolysis of slowly biodegradable substrate, which occurs under aerobic conditions.
2. Anoxic hydrolysis of slowly biodegradable substrate that takes places in anoxic circumstances.

Anaerobic hydrolysis of slowly biodegradable substrate which describes the hydrolysis process in an anaerobic environment.

The hydrolysis of the slowly biodegradable substrate, the aerobic degradation of the fermentation products and the substrates (aerobic growth), the anoxic oxidation of the fermentable organics (S_F) and fermentation products (S_A), the reduction of nitrate S_{NO3} (denitrification), and the anaerobic fermentation of the fermentable organics to fermentation products are all carried out by the heterotrophic organisms. These organisms are also susceptible to lysis and degradation.

4. and 5. Heterotrophic organisms develop aerobically on fermentable substrates and fermentation products. The two degradable organic substrates S_F and S_A are consumed in these two processes, that were considered parallel processes.

6. and 7. The heterotrophic organisms undergo anoxic growth on fermentable substrates and on fermentation products accompanied by denitrification. These are comparable to the two aerobic growth processes, however nitrate, S_{NO3}, is needed as the electron acceptor as opposed to oxygen.

8. Fermentation of heterotrophic organisms that is supposed to proceed in anaerobic conditions in which fermentation products S_A are obtained from the readily biodegradable substrate S_F.

9. Lysis of heterotrophic organisms in which all decay and loss processes are considered that relate to the heterotrophic organisms.

The phosphorus-accumulating organisms (X_{PAO}) are known to have the ability to store phosphorus as poly-phosphate X_{PP}. The capability of certain phosphorus-accumulating organisms, or PAO, to denitrify has been demonstrated, contrary to earlier assumptions that they couldn't. This major objection, that PAO considerably contribute to denitrification, which is not specified in ASM2, has been addressed with the advent of ASM2d. In this model (ASM2d) it is considered that processes involving PAO occur in both aerobic and anoxic circumstances. However, their growth is limited to the cell internal organic materials (X_{PHA}).

10. In order to store cell external fermentation products S_A in the form of cell internal organic storage material X_{PHA}, it is hypothesized that PAO may release phosphate, S_{PO4}, from poly-phosphate, X_{PP}, and use the energy that becomes available from X_{PP}'s hydrolysis.

11. and 12. Polyphosphate is stored in both aerobic and anoxic conditions. Energy for the PAO can be obtained from the aerobic or anoxic respiration of X_{PHA} in order to store ortho-phosphate, S_{PO4}, in the form of cell internal polyphosphates, X_{PP}.

13. and 14. Growth of phosphorus-accumulating organisms under anoxic and aerobic conditions. These organisms are thought to only grow by use of the cell internal organic storage products (X_{PHA}). It is reasonable to suppose that the organisms utilize ortho-phosphate, S_{PO4}, as a nutrient for the synthesis of biomass since phosphorus is continually produced by the lysis of X_{PP}.

15., 16. and 17. All PAO fractions are lost or decay as a result of death, endogenous respiration, or maintenance.

In terms of the nitrification process, the transformation of ammonium to nitrate is considered to occur directly, in a one-step process while nitrite, as the intermediate compound, is not taken into account as a component for the model.

18. The nitrifying organisms grow in aerobic environment by consuming ammonium as nutrient and substrate resulting in the production of nitrates. This nitrification process also reduces the alkalinity.

19. The lysis of nitrifiers is modelled analogously to the lysis of heterotrophic organisms and to ASM1.

The last two processes integrated in the ASM2d describe the chemical precipitation of phosphates. In biological nutrient removal systems, naturally occurring metals in the wastewater, e.g., such as Ca^{2+}, and the high concentration of released soluble ortho-phosphate, S_{PO4}, may cause phosphorus to chemically precipitate (e.g., as apatite or calcium phosphate). Another widely used method for removing phosphorus is simultaneous precipitation of phosphorus with the addition of iron or aluminium salts. Biological phosphorus removal may be combined with simultaneous precipitation if the carbon to phosphorus ratio is unfavourably low.

20. And 21. The basis of the precipitation model is the presumption that precipitation and redissolution are opposing processes that, at steady state, are in balance with each other as described in the equilibrium reaction Eq. (1.1).

$$X_{MeOH} + S_{PO4} \leftrightarrow X_{MeP} \quad (1.1)$$

The following reaction rates may be applied in order to model the precipitation and redissolution processes:

$$rate_{20} = k_{PRE} \cdot S_{PO4} \cdot X_{MeOH} \quad (1.2)$$

$$rate_{21} = k_{RED} \cdot X_{MeP} \quad (1.3)$$

In case the processes are in equilibrium, the equilibrium constant may be written as:

$$K_{eq} = \frac{S_{PO4} \cdot X_{MeOH}}{X_{MeP}} \quad (1.4)$$

1.3. Artificial neural network models [14]

Artificial neural networks are parallel distributed processors made up of basic processing units called neurons that are modelled after the natural neural systems. ANNs fall under the category of machine learning models that have high generalization and learning capabilities for a range of classification, prediction, and modelling tasks [15].

The basic building block of an artificial neural network, i.e., the neuron, is illustrated in a general form in Figure 1.4. The input data (p) is conveyed by a connection which multiplies it by a weight (w). The bias (b), which has a constant value of 1, is then added to the product of the previous multiplication to form the

net input (*n*). The net input is further transmitted to become the argument of a transfer function (*f*), that is usually a step function or some sort of sigmoid function, which produces the output of the neuron (*a*).

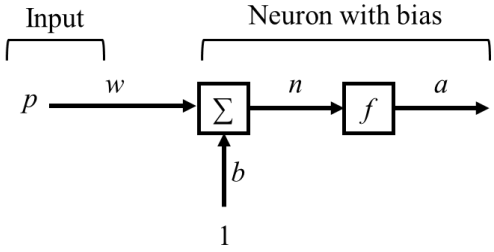

Figure 1.3 Schematic of a neuron with bias

The neuron can also have several inputs at the same time, or a vector of input data. In this case each of the inputs is transmitted through a separate connection with its own distinct weight as illustrated in Figure 1.4. As such, the net input will be calculated as the dot product of the weights and inputs also shown in Eq. (1.5).

$$n = w_{1,1}p_1 + w_{1,2}p_2 + \cdots + w_{1,N}p_N + b \tag{1.5}$$

where N is the number of elements in the input vector.

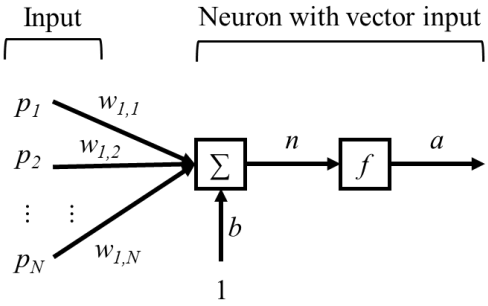

Figure 1.4 Representation of a neuron with multiple inputs

Several neurons can be employed in order to create a layer of neurons. An artificial neural network is made up of one or more layers like the one illustrated in Figure 1.5. The number of neurons in the layer is noted by L, and it can be observed that in case of multiple layers the input information is transmitted through a weight matrix with L rows and N columns. The indices in the matrix show the source and destination of the information, i.e., from element N to neuron L. In this case, it can be seen that the layer of neurons will provide a vector of outputs consisting of L elements.

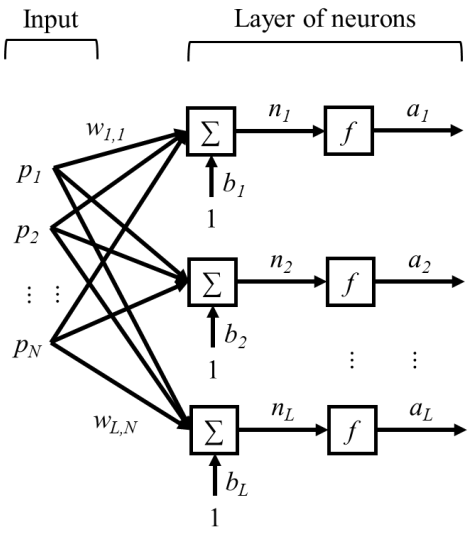

Figure 1.5 Illustration of a neuron layer

As previously mentioned, an ANN can be created by connecting multiple such layers of neurons, e.g., the three-layer network presented in Figure 1.6. In this case a notation will be added to all the architecture elements in order to keep track of which layer they belong to. This allows for each layer to be treated as a separate single-layer network. The final layers where the outputs of the ANN are computed is usually referred to as the output layer, whereas the others are known as hidden layers. The first two layers (Layer 1 and Layer 2) of the illustrated ANN are hidden layers, while the last layer (Layer 3) is the output layer.

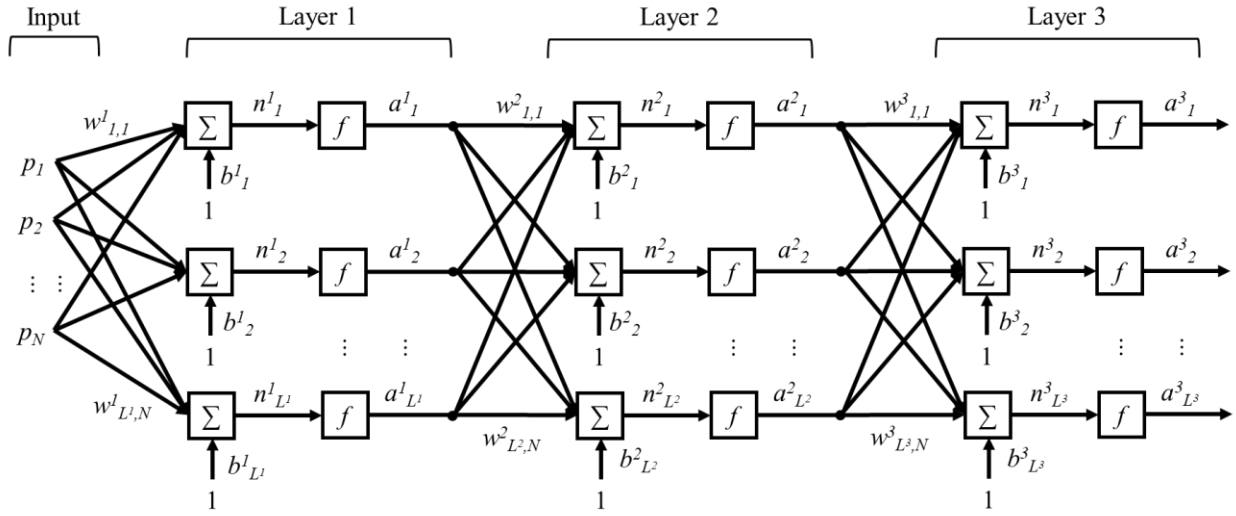

Figure 1.6 Architecture of a three-layer ANN

1.4. Goal and objectives

The scope of this thesis is the assessment and optimization of the performance of various wastewater treatment technologies and strategies applied to the energy intensive urban wastewater treatment processes by employment of artificial intelligence (AI) techniques, aiming for potential energy efficiency improvements, cost and GHG emissions reduction. The following is a list of the objectives to be met in order to accomplish the intended goals:

1. A thorough review of the literature to grasp the current state of research and state-of-the-art technologies.
2. Development of AI models for various wastewater treatment plant configurations and control strategies in order to obtain a swiftly operating model that can be further employed in optimization of the wastewater treatment process in terms of environmental and economic improvements.
3. Optimization of AI model fidelity through the study of the model architecture, in the case of artificial neural networks (ANNs), by searching for the best hyperparameter values via both full factorial and genetic algorithm optimization processes.
4. Simulation and optimization of existing and proposed control strategies related to energy efficiency, GHG emissions, effluent quality, and overall cost taking into account several WWTP system configurations by the use of the developed AI models.
5. Development of ANN models for detection and identification of sensor fault types aimed at the DO sensor in order to ensure the proper operation of the WWTP by avoiding degradation in effluent quality or increase in energy consumption due to the prompt detection and identification of defects.

WWTPs account for 1-2% of overall GHG emissions with an upward trajectory [16], leading to an increase in attention on the subject of global warming [17]. Of the three main gases the biological treatment is responsible for the majority of CH_4 and N_2O emissions, while the non-biogenic CO_2 emissions are related to the plant's energy consumption and chemical use [18]. Regarding the biogenic CO_2 emissions, these are not to be taken into consideration for the GHG emission inventories [19] although this could lead to under-estimation of GHG emissions from WWTPs [20]. The biological treatment can also reach energy consumption of 50% to 70% of the WWTPs energy demand, in case of plants in China [5]. At the same time, the largest share of the plant carbon footprint, i.e., up to 78.4%, can be attributed to N_2O emissions [21]. As such, the denitrification process, namely the aeration process, plays an essential role in the optimal operation of the WWTP and the studies on the influence of DO on plant operation have grown in popularity [22].

Another important aspect in maintaining a sustainable operation is the sensor malfunctions as these bring forth enormous disruptions in process control and energy efficiency [23]. These sensor faults may arise as a result of harsh environmental conditions, electrical failure, or even incorrect calibration [24], and their timely detection is essential in mitigating the potential impact of these malfunctions and in maintaining process integrity [25].

The amount of wastewater is expected to grow concurrently with the population and economy, while standards for the effluent waters are expected to become more stringent that would also lead to an increase in GHG emissions [26]. Taking all of the above into consideration, the following case studies were selected:

1. Recycle rate flowrate optimization for WWTP waterline
2. Control loop setpoint optimization for WWTP waterline
3. Air flowrate optimization for WWTP waterline
4. Seasonal DO setpoint optimization for full scale WWTP
5. Detection and identification of DO sensor fault types

2. WWTP simulation and performance assessment methods

A benchmark simulation environment was needed to be defined for simulation-based evaluation of the proposed strategies for the WWTPs. The development of the benchmarks pursued to combine simplicity with reality and conventional standards. The purpose of these simulation models was that, once validated, the proposed control strategy could be employed and evaluated by a well-defined set of criteria. Over the years several such Benchmark Simulation Models (BSMs) were developed.

2.1. WWTP simulation with BSM1

The first benchmark simulator considers a relatively simple plant layout focused entirely on the water-line of the WWTP (Figure 2.1). The system consists of a five-compartment bioreactor with anoxic-oxic configuration employing the ASM1 for the modelling of process variables, also known as AO, followed by a secondary settler (clarifier) modelled using the double-exponential settling velocity function proposed by Takács *et al.* [59]. Of the five reactors the first two are considered the anoxic reactor, while the latter three reactors are aerated via compressed air. This is one of the common approaches for biological nutrient removal combining the nitrification and predenitrification processes, which is also frequently employed at full-scale WWTPs. For the description of the biological processes taking place in the reactors the ASM1 was adopted.

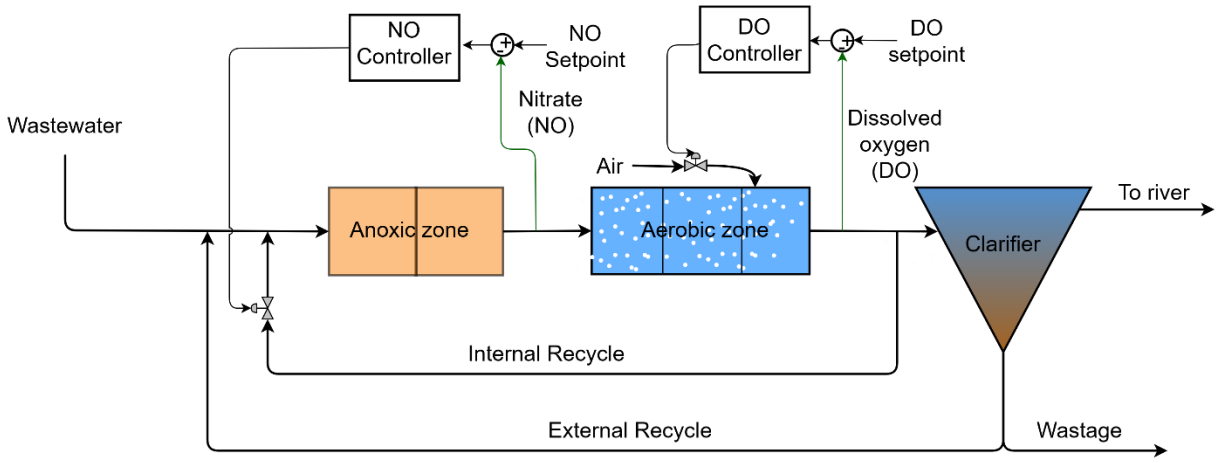

Figure 2.1 BSM1 plant general overview

Although the BSM1 provides a commonly adopted approach to wastewater treatment systems and lays the groundwork for a realistic description of a full-scale WWTP, not all plants employ the presented

method. This is also the case at the local municipal plant, where an A^2O or anaerobic-anoxic-oxic layout is employed for the bioreactors. The anoxic-aerobic method utilized in the BSM1 layout enables the plant to meet stringent COD and total nitrogen removal requirements, whereas the A^2O strategy is designed for fulfilling not only carbon and total nitrogen regulation limits, but also other nutrient removal requirements which are not considered in the classic ASM1 model such as total phosphorous. In terms of plant layout, the difference between the methods is the connection of the internal recycle stream. It can be observed that in the BSM1 layout both recycle streams are connected to the influent wastewater, while in the case of an A^2O treatment method the internal recycle streams connects between the first and second bioreactor (Figure 2.2).

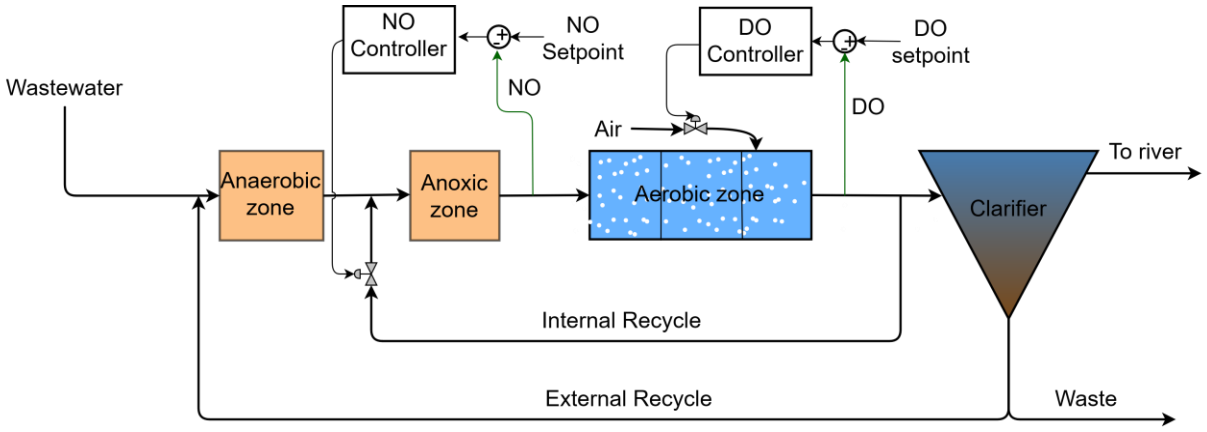

Figure 2.2 General overview of WWTP employing A^2O treatment method

When trying to adapt and calibrate the BSM1 based on data from the local municipal WWTP rather than the slight modification to the plant layout, the calibration of stoichiometric and kinetic parameters describing the biological processes poses a much greater challenge. The impressive work of calibrating the BSM1 model was achieved by a fellow PhD student, Melinda Simon-Várhelyi, and further information on this topic can be found in their research [27].

Relating to the control utilized in the BSM1 layout it can be observed that two PI control loops are employed. The first regulates the nitrates and nitrites concentration in the effluent of the second reactor by manipulating flowrate of the internal recycle stream based on the nitrates and nitrites concentration in the effluent of the second reactor. While the second control loop is responsible for the dissolved oxygen level in the effluent of the fifth bioreactor by acting on the air flow going to the latter three reactors based on the dissolved oxygen level in the effluent of the fifth bioreactor.

2.2. WWTP simulation with BSM2

The Benchmark Simulation Model No. 2 was developed with the concept of a long-term and plant-wide model. This was a necessary extension as one of the shortcomings of the BSM1 was that a thorough long-term evaluation of the plant operation or different control strategies required a longer evaluation period. The BSM1 plant configuration was updated with wastewater pre-treatment in the water-line and with the sludge-line processes including anaerobic digestion. The extended evaluation period allows for a more in-depth assessment of plant operation and control strategies by allowing the processes with slow dynamics to also be considered.

The BSM2 includes a primary clarifier situated before the activated sludge reactors which is described by the Otterpohl model [28]. In order to model a full-scale WWTP, the BSM2 model also contains a sludge thickener, an anaerobic digester, a dewatering system, and a storage tank as can be observed in Figure 2.3.

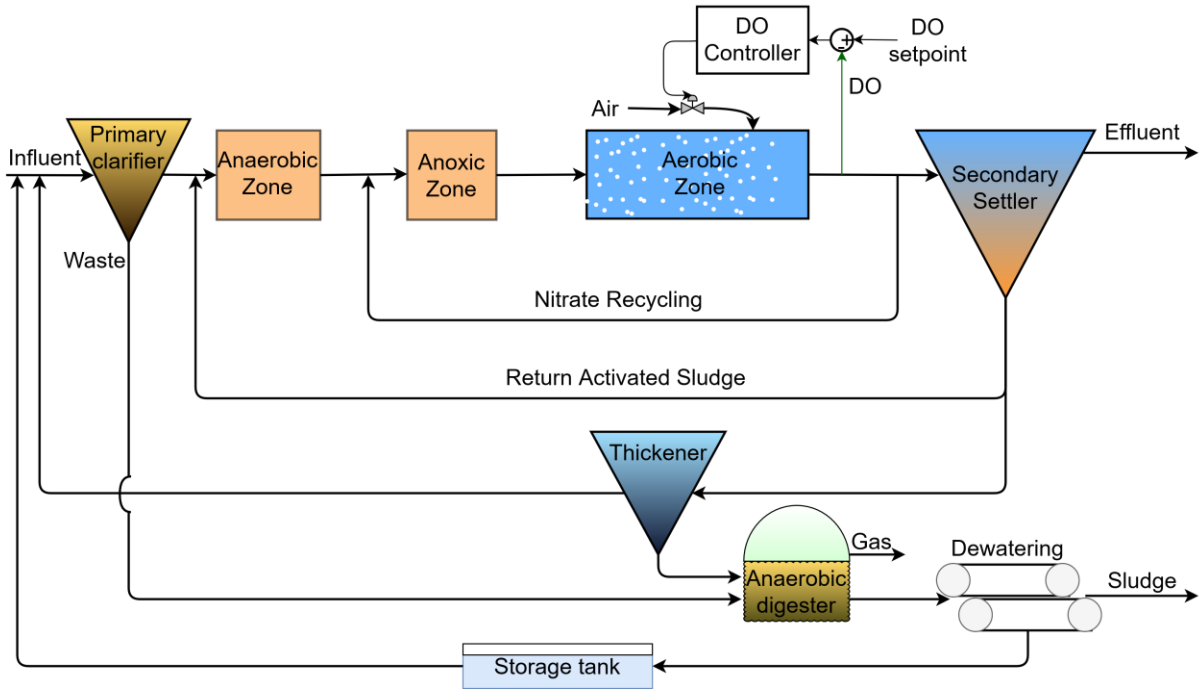

Figure 2.3 Schematic representation of the BSM2 plant

2.3. Matlab/Simulink

Matlab is both a programming language and numerical computation environment, which offers tools for algorithm implementations, manipulation of matrices and also various plotting possibilities of functions and data. Simulink is a block diagram programming environment which is integrated with Matlab, and

among its numerous applications its main uses are modelling and simulation of dynamic systems, and continuous test and verification systems.

In most cases Matlab and Simulink are employed together allowing the combination of text-based and graphical programming for the development and simulation of envisioned systems. This is achieved by incorporating algorithms created in Matlab into Simulink model blocks that can be used alongside the default blocks available in the library, and at the end of the simulation the results can be exported to Matlab workspace for further use. In order to implement an algorithm aimed to build a process model and to add it as a Simulink model it has to be structured into an S-function. System-functions or S-functions represent a powerful method to augment the Simulink environment. A template has to be used when implementing an algorithm to reach the general form of an S-function. This general form of the S-function defines the blocks behaviour in each of the simulation steps that are initialization, update, derivatives computation, update of states and outputs, and termination. Figure 2.4 illustrates a Simulink block consisting of sets of input, states, parameters and output variables/sets.

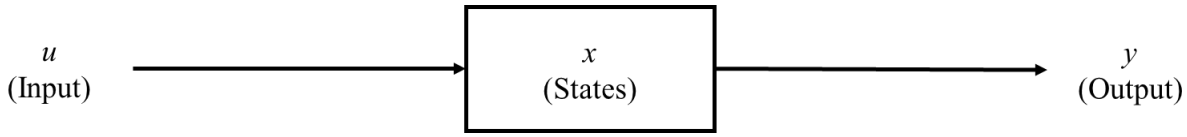

Figure 2.4 Representation of a Simulink block

2.4. WWTP operation evaluation

Data analysis is mandatory to assess the performance and potential of WWTP operation strategies. The BSM technical reports describe evaluation methods that were designed to combine the large amount of output data into a few geographically independent composite terms [29]. These criteria make the objective and simple comparison of the impact of various operation strategies possible. The composite terms described below were employed for operation evaluation in all of the case studies presented in Chapter 3, namely the effluent quality index, aeration energy, and pumping energy.

The effluent quality index (EQI) (kg pollution unit/day, kg_{PU}/d) evaluates the daily released mass of pollutants by taking into account the effluent values of TSS (PU_{TSS}), COD (PU_{COD}), BOD (PU_{BOD}), total Kjeldahl nitrogen (TKN) (PU_{TKN}), nitrate and nitrite (NO) concentration (PU_{NO}) and by also considering the effluent flow rate (Q_e) as shown in Eq. (2.1).

$$EQI = \frac{1}{1000 \cdot T} \cdot \int_{t_i}^{t_n} [PU_{TSS}(t) + PU_{COD}(t) + PU_{BOD}(t) + PU_{TKN}(t) + PU_{NO}(t)] \cdot Q_e(t) dt \quad (2.1)$$

The calculation of the aeration energy index AE (kWh/d) takes into account the oxygen transfer coefficient (K_La), the volumes of the aeration tanks (V) and the saturated oxygen concentration (SO_{sat}).

$$AE = \frac{SO_{sat}}{1.8 \cdot 1000 \cdot T} \cdot \int_{t_i}^{t_n} \sum V \cdot K_L a(t) dt \quad (2.2)$$

While the pumping energy index PE (kWh/d) is computed based on the internal recycle flowrate (nitrates recycle) (Q_{NR}), the external recycle flowrate (return activated sludge recycle) (Q_{RAS}) and the flowrate of waste (Q_W). These values are averaged over the period of observation T (from t_i to t_n).

$$PE = \frac{1}{T} \cdot \int_{t_i}^{t_n} [0.004 \cdot Q_{NR}(t) + 0.008 \cdot Q_{RAS}(t) + 0.05 \cdot Q_w(t)]dt \quad (2.3)$$

2.5. ANN modelling and evaluation

2.5.1. Studied artificial neural network types

Multiple ANN types were investigated in order to determine the most suitable network for predictions. Throughout the case studies four types, that can be categorized in two classes, of ANNs were explored to discover the most appropriate one, in terms of training time and prediction accuracy assessment criteria. One of the classes was the nonlinear autoregressive network with exogenous inputs (NARX), while the other was the class based on the use of radial basis functions simply called the Radial Basis Function (RBF) networks.

The tapped delay line block between the ANN model time-series inputs and the first hidden layer is used in the design of the NARX type of feed-forward neural network to provide the ANN models a strong memory feature characteristic. This line enables the prediction of the target variable value at the proximate sampling moment of time using data from previous time moments in case of both the input and the target datasets.

The four types of considered ANNs were: the “open” structure of the NARX class also known as Time Delay Neural Network (TDNN); the “closed” NARX structure, usually referred to as Recurrent Neural Network (RNN); and the Radial Basis Neural Network (RBNN) and Generalized Regression Neural Network (GRNN) that are part of the RBF class. These four types were selected as NARX type networks that are well-known for their use in time series modelling, and as RBF type ANNs, i.e., RBNN and GRNN that have also been effectively utilized in time series prediction studies [30].

TDNNs type comprises the feed-forward neural network with a tapped delay line block between the inputs and the first hidden layer which enables the networks to operate with data from previous time moments. RNNs are built similarly to the TDNNs mentioned previously. The tapped delay line is also present in these networks. In this case the output values are directly connected by feedback from the network’s own previously computed outputs.

RBNNs were developed with two layers: a hidden layer called radial basis layer as the first layer, and a linear output layer as the second. As the default RBNN does not contain the tapped delay line in its architecture, the function of such a line was replicated by manually adding the data from previous time

moments as input to the network. The GRNNs, similarly to the RBNNs, had two layers in their construction. For the GRNN models, the time delay was also manually added. The first layer operates similarly to the first layer in RBNNs, while the second layer –known as the special linear layer– represents the difference between the two ANN types.

2.5.2. ANN evaluation criteria

It is imperative for the best designed and trained ANN models to be selected for further use. In order to achieve this, their performance has to be assessed. For this purpose, a total of three criteria were used. The first is the coefficient of determination (R^2), which has an ideal value of 1, measures how well can the model outcomes predict by assessing the goodness-of-fit between the predicted and targeted values. The calculation of this criterion is shown in Eq. (2.4).

$$R^2 = 1 - \frac{\sum_{i=1}^{N}(y_i - x_i)^2}{\sum_{i=1}^{N}(y_a - y_i)^2} \tag{2.4}$$

where y_a is the average value of the target data, y_i is the desired output at data point i, x_i is the model output at data point i, and N is the number of observations.

The second criterion used in the assessment of ANN models was the mean squared errors (MSE), which calculates the squared errors between each targeted and predicted pair of values and provides the average of these squared errors. The MSE is calculated as follows:

$$MSE = \frac{1}{N}\sum_{i=1}^{N}(y_i - x_i)^2 \tag{2.5}$$

The last criterion, the mean absolute percentage error (MAPE). This criterion's value is the average of the absolute percentage errors between the targeted and predicted values, with the absolute errors' division to the targeted value used to convert them to percentages. The MAPE criterion was computed based on Eq. (2.6).

$$MAPE = \frac{\sum_{i=1}^{N}\frac{|y_i - x_i|}{y_i}}{N}100 \tag{2.6}$$

3. WWTP operation enhancement investigated cases

3.1. Optimization of WWTP waterline recycle flowrates

In the first case study a control system consisting of the DO control loop was considered for the automated control of the air flowrate in the bioreactors. The return activated sludge and nitrate recycling streams were controlled as a given ratio to the influent flowrate (Fig. 3.1.), which is a commonly adopted approach in facilities lacking the NO control loop. The current study aimed to develop accurate neural network dynamic models, by exploring four types of ANN architectures, that are further used in the optimization of the recycle flowrates and thus the WWTP operation. The main steps of the presented research are:

- Data generation using a mathematical model based on ASM1 and calibrated on plant data.
- ANN development and selection of most accurate ANN models for the novel approach of directly modelling the WWTP performance indices.
- Optimization of the control system gains that manipulate the nitrate recycling and the return activated sludge flowrates in a specified ratio to the WWTP influent flowrate, based on an objective function which considers environmental and energy performance indices.

The layout of the municipal WWTP used as case study is presented in Figure 3.1. It has an anaerobic-anoxic-oxic (A^2O) configuration and uses a feedback control loop for plant aeration, while the two recirculation flowrates are determined by multiplying the inlet flowrate with separate gain factors [31]. The feedback control loop is responsible for the nitrification process by controlling the DO level in the aerated reactors and manipulating the air flowrate [32]. A 7 days period that was representative for the whole dataset was selected and used for different recirculation gain simulation scenarios.

All four network types presented in Section 2.5.1 were investigated with the aim of finding the most suitable network to be used for predictions. The inputs of the studied ANNs consist in the past and present values of the following influent variables: COD, ($NH_4^+ + NH_3$) nitrogen concentration, volumetric flow (Q), temperature, and the two gain factors (K_1 and K_2). Additionally, depending on the type of network (single output - MISO or multiple output – MIMO), the ANN input also contains the past values of the increments (from one sampling time to the next one) of one or more performance indices. The performance indices were calculated as described by equations (2.1), (2.2), and (2.3).

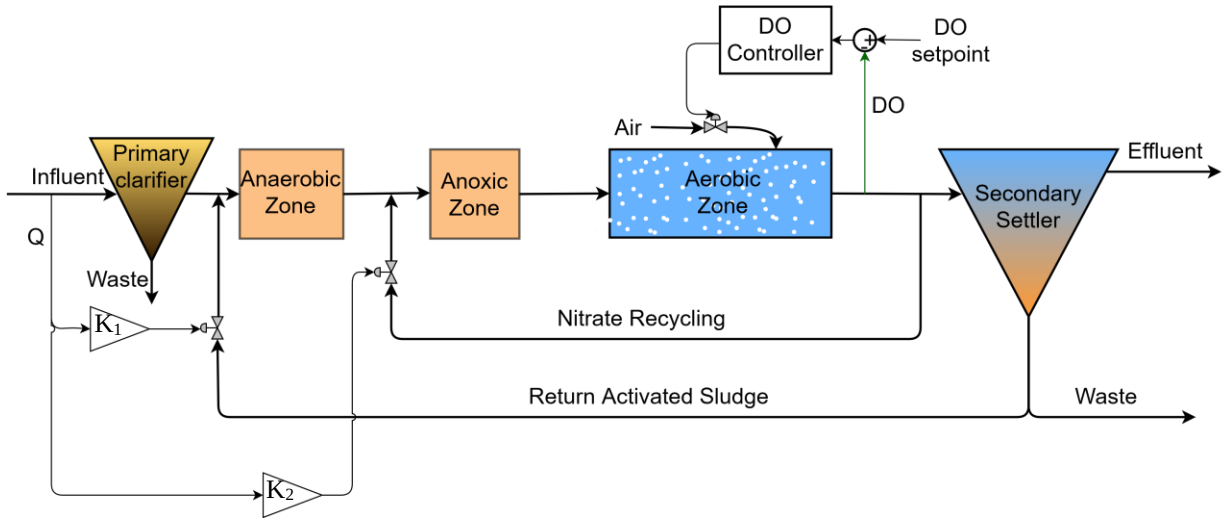

Figure 3.1 Schematic representation of studied WWTP and its control system

The decision variables for the current problem were the two gain factors controlling the external and internal recycle flowrates. Both MISO and MIMO model structures were further employed for the optimization of a 7-day period scenario with the following objective function:

$$f_{min} = AE + 8 \cdot EQ + PE \tag{3.1}$$

The best networks of each topology obtained from the trial-and-error process were used for prediction of a 7 days long period, considering a not yet seen scenario of ANN inputs. The MAPE values and other ANN performance results, obtained with the selected best networks, are presented in Table 3.1.

Table 3.1 Test and prediction results for the best MISO and MIMO networks

ANN type	Transfer functions		Output	Testing		Prediction			Avg. training time (s)
	Hidden layer 1	Hidden layer 2		R^2	MSE	R^2	MSE	MAPE	
TDNN	logsig	tansig	ΔAE/MISO	1	2.27E+04	0.99	1.05E+05	1.19	5.7
RNN	logsig	-	ΔEQ/MISO	1	2.52E+04	0.89	1.41E+06	3.50	600
RNN	logsig	-	ΔPE/MISO	1	3.66E+02	0.99	5.00E+02	0.85	30
RNN	logsig	logsig	All/MIMO	1	5.31E+04	0.99	5.11E+05	2.39	52

The previously presented best trained networks were further used for the optimization of the standard scenario spanning over 7 days. The optimization results are presented in . All of the model structures reduced the nitrates gain from the actual operational practice (reference case) value of 0.8 value to a value around 0.62.

Table 3.2 Optimization results

	Nitrates gain (K_2)	Activated sludge gain (K_1)	AE (kWh/d)	EQ (kg_{PU}/d)	PE (kWh/d)	Optimization time (s)
Reference case	0.80	1.00	1.76E+04	1.67E+04	1.26E+03	-
Analytical	0.65	0.80	1.71E+04	1.66E+04	1.03E+03	16724
MIMO	0.62	1.07	1.71E+04	1.68E+04	1.12E+03	0.97
MISO	0.60	0.99	1.70E+04	1.68E+04	1.07E+03	2.24

By analysing prediction accuracy and optimization results of the developed ANN models for WWTP operation improvement by internal and external recycle flowrate optimization, it can be concluded:

- The optimizations conducted for a 7-day time period showed that the performance indices AE and PE were successfully predicted with the small MAPE values of about 1%.
- The optimal solutions found by both ANN model structures resulted in the reduction of the two performance indices compared to the reference case.
- An important advantage was observed at the computation time for the optimization task, between using the ANNs (0.97 and 2.24 seconds) versus the analytical model (16724 seconds) for optimization.

3.2. Optimization of WWTP waterline control loop setpoints

The second case study investigated the optimization of the control system that had both the DO and NO automatic control systems. This current work consisted in a thorough ANN development directly predicting the WWTP performance indices, and aimed to find the most suitable type, design, and training methodology of the ANNs for building of highly accurate dynamic models. They were further used in the WWTP operation optimization for finding the best setpoint values of the main control loops responsible for the carbon oxidation, nitrification, and denitrification essential WWTP sub-processes (Figure 3.5). The main steps of the presented work are:

- Generation of two representative data sets, one smaller (screening) and one larger, using the calibrated analytical model and the design of experiments algorithms, with the aim of collecting a minimum but rich enough set of data for achieving an effective and efficient training procedure.
- Based on the small screening dataset, the selection of the best performing ANN structure and type was performed by evaluating the prediction accuracy and time requirements for training

four types of ANN models aiming to describe the WWTP dynamic behaviour of the effluent quality variables.

- Based on the screening step results and using the larger dataset a new training and selection of the highest-performing ANN type and architecture was carried out for building new ANN models, able to accurately describe the performance indices of the WWTP, and considering their further use in the optimization step.
- Optimization of the WWTP operation based on the best performing ANN models that predict the WWTP energy and effluent quality indices, to find the most favourable setpoint values for the Dissolved Oxygen and Nitrate and Nitrite concentration control loops.

Plant data was collected from the WWTP influent and process variables measurements, considering a sampling period of 30 minutes and for a period of 22 days. The layout of the municipal WWTP used as case study is presented in Figure 3.2.

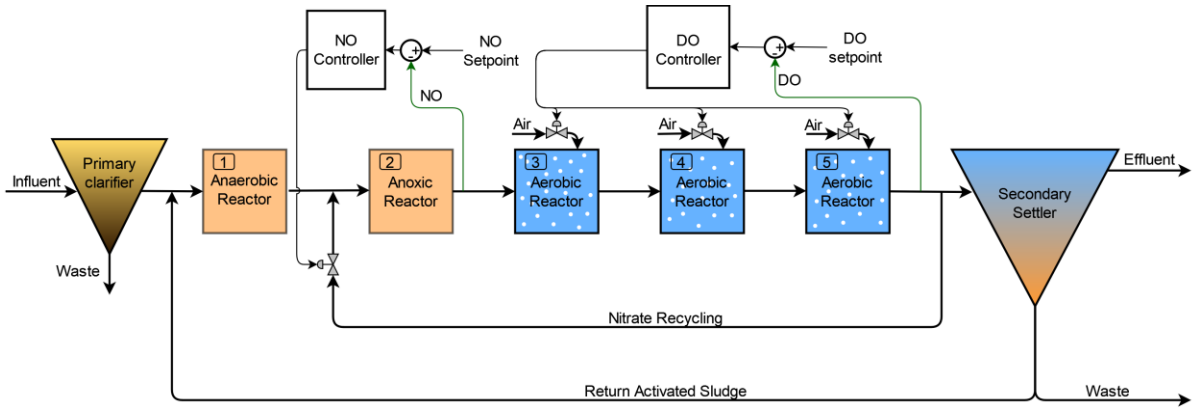

Figure 3.2 Schematic of studied WWTP layout and its control system

The current study employed all of the presented ANN types mentioned in Section 2.5, and the considered network hyperparameters were almost identical to the ones studied in the previous case study. For the new batch of networks, the influence of the length of the tapped delay line time-horizon on the ANN prediction accuracy and training duration was also investigated. Values between 12 and 100 were considered for this ANN model parameter.

A period of 7 days was selected for the optimization process. The most efficient ANNs for predicting the WWTP indices were selected, both for the MISO and the MIMO structures, in order to find the optimal setpoints for the control loops (NO_{ref} and DO_{ref}) considering the ranges presented in Table 3.3 and the objective function presented in Eq. (3.2).

$$f_{min} = AE + 4 \cdot EQ + PE \tag{3.2}$$

Table 3.3 Range of values for the control loops setpoints

Variable	min	max
NO_{ref} (mg N/L)	0.005	0.02
DO_{ref} (mg O_2/L)	1	3

The best models for each output feature at the screening step are presented in Table 3.4. These types of models were further considered in the final selection step, where the larger dataset was utilized in their development and the trade-off between prediction accuracy and training time was considered by increasing the time horizon of the tapped delay line. The obtained results are presented in Table 3.5.

Table 3.4 Testing and prediction results of best networks for each output feature at the screening step

ANN type	Transfer functions		Output	Testing		Prediction (Second testing)		Avg. training time (s)
	Hidden layer 1	Hidden layer 2		R^2	MSE	R^2	MSE	
GRNN	radbas	-	TSS	0.89	1.81E-02	0.54	2.90E-01	0.074
TDNN	tansig	-	COD	1.00	7.92E-04	0.77	2.42E-01	0.56
RNN	logsig	tansig	BOD	0.88	2.97E-04	0.72	1.82E-02	202
TDNN	tansig	logsig	TKN	1.00	6.31E-05	0.87	1.14E-02	0.48
GRNN	radbas	-	NO	0.96	1.13E-02	0.77	1.07E-01	0.071
RBNN	radbas	-	All	0.99	2.43E+07	0.98	2.82E+07	4.8
RBNN	radbas	-	EQ	1.00	4.53E+04	0.76	1.84E+07	2.3

The results of the optimization performed with the ANN models highlighted in Table 3.5 for the control loop setpoints, computation time, and values of the performance indices obtained with the optimal setpoints are presented in Table 3.6.

The following conclusions were be drawn by assessing the two-step ANN model development and optimization results:

- The screening step revealed that networks trained directly with the EQ as single output variable presented higher potential for making effective predictions, and RNN networks with two hidden layers were the least promising.
- The increase in length of the tapped delay line showed positive influence on the accuracy of RBNNs, while TDNNs showed a nonuniform response.
- The optimization of control loop setpoints led to the enhancement of WWTP operation by a decrease of 1303 kWh/day in terms of energy consumption and a decrease of 324 kgPU/day in terms of effluent quality index.

- The MIMO ANN model performed the optimization task about 180 times faster when compared to the analytical model based optimization.

Table 3.5 Influence of varying the tapped delay line horizon length on the prediction accuracy and training time at the ANN final selection step

ANN type	Output	Delay horizon	R^2	MSE	MAPE (%)	Training time (s)
RBNN	AE	12	0.95	2.06E+05	1.79	100
RBNN	AE	25	0.95	1.62E+05	1.54	190
RBNN	**AE**	**50**	**0.97**	**9.37E+04**	**1.27**	**700**
RBNN	AE	100	0.96	1.16E+05	1.33	2300
TDNN	EQ	12	0.97	3.92E+05	3.09	130
TDNN	EQ	25	0.94	1.38E+06	5.36	170
TDNN	EQ	50	0.92	8.40E+05	4.20	180
TDNN	**EQ**	**100**	**0.98**	**3.73E+05**	**2.57**	**550**
TDNN	**PE**	**12**	**0.98**	**8.66E+02**	**1.51**	**31**
TDNN	PE	25	0.84	5.95E+03	4.04	34
TDNN	PE	50	0.98	7.21E+02	1.58	56
TDNN	PE	100	0.98	1.10E+03	1.76	330
RBNN	All	12	0.99	3.48E+05	2.91	71
RBNN	All	25	1.00	3.42E+05	2.99	150
RBNN	**All**	**50**	**1.00**	**2.28E+05**	**2.37**	**500**
RBNN	All	100	1.00	2.62E+05	2.64	2600

Table 3.6 Optimization results with the best ANN and FPM used for AE, EQ, and PE computation

Model	NO setpoint (mg N/L)	DO setpoint (mg O_2/L)	AE (kWh/day)	EQ (kg_{PU}/day)	PE (kWh/day)	Optimization time (min)
Base case	1.00E-02	2.000	17646	16575	1381	-
FPM	5.00E-03	1.422	16218	16243	1351	423
3 MISO ANN	5.00E-03	1.251	15899	16357	1427	2.04
MIMO ANN	5.50E-03	1.487	16366	16251	1358	2.34

3.3. Optimization of WWTP air flowrate distribution

The third case study investigated the optimization of the airflow distribution to the aerated reactors. This study aims to find optimal aeration parameters (i.e., three gain factors steering the air flowrate distribution) for an operation strategy of the aeration unit-process conducting to an optimized distribution of air flow to the aerated bioreactor, and to evaluate it in terms of energy consumption, effluent quality, and GHG emissions. In the current study GHG emissions were considered for the biological reactors and associated settlers of the water line, as they represent the most important source of GHGs. The computation of the optimal operation parameters for the proposed aeration strategy was relying on the predictions of the WWTP energy performance indices, effluent quality, and GHG emissions using dynamic hybrid intelligent models developed on the basis of simulated datasets. These dynamic neural network NARX models, for which the optimal topology was searched for by means of GA will be further referred to as GA-NARX. To the authors' knowledge, there are no studies associated with hybrid intelligent modelling based on GA optimized NARX models, aimed at simulation of the WWTP processes. Furthermore, the dynamic modelling of GHG emissions in WWTPs by means of ANN models is also a novelty of the present work. The main steps of the current study were:

- Generation of the representative dataset by using the calibrated analytical model of the municipal WWTP considered as case study, and by taking into account the specifically and multiple designed scenarios of operational parameters.
- Development of GA-NARX methodology for searching the optimal ANN topology in terms of structure of NARX network at training, number of hidden layers (NHL), number of neurons in each hidden layer (NNeHL), and transfer functions (TFs).
- Employment of the ANN developed models in a multi-objective optimization step for finding the optimal operational aeration parameters.

Testing the optimal operational parameters on the analytical model and comparison of energy consumption, effluent quality, and GHG emissions performance with the standard WWTP operation.

An analytical model based on Activated Sludge Model No. 1 was utilized for the generation of the dataset required for the development of GA-NARX models. For each of the aerated reactors the air flowrate can be distributed unevenly using three gain factors (G1-G3), as can be observed in Figure 3.3.

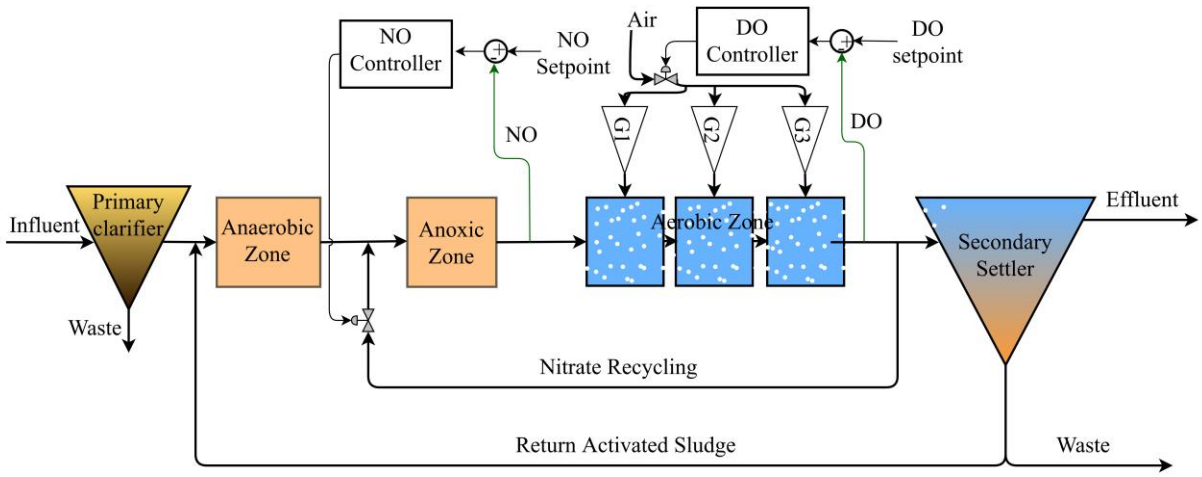

Figure 3.3 Schematic representation of the studied WWTP

Population-based algorithms, such as GAs provide appropriate means for finding the global optimum in the ANN architecture optimization [33]. ANN models with 1 or 2 hidden layers were considered, with NNeHL between 2 and 15. TFs at each hidden layer were chosen as a logsig or a tansig function.

Evaluation of the GHG emissions was performed at the water line level of the WWTP, considering both on-site and off-site emissions of CO_2 and N_2O, as described in equations (3.3)-(3.7). The assessment of the on-site CO_2 emissions was calculated in (kg CO_2/m^3 WW), based on the relationship described in Eq. (3.3) [34].

$$P_{CO_2,on-site} = \left(0.99 \cdot (1 - Y_H) \cdot \eta_{ASP} \cdot bCOD + 1.03 \cdot Y_H \cdot \eta_{ASP} \cdot bCOD \cdot \frac{k_{d,H} \cdot MCRT}{1 + k_{d,H} \cdot MCRT}\right) \quad (3.3)$$

here, 0.99 (kg CO_2 eq./kg COD) is the emission factor corresponding to organic compounds, Y_H is the heterotrophic biomass yield in (mass VSS/mass COD), η_{ASP} refers to the removal of biodegradable COD (*bCOD*) in the activated sludge reactors, 1.03 (kg CO_2 eq./kg COD) is an emission factor in relation to the activated sludge biomass, $k_{d,H}$ is the decay rate for heterotrophic biomass with a value of 0.3 (d^{-1}) [35], and *MCRT* is the mean cell retention time, taken as 15 days for the current municipal WWTP case.

The on-site N_2O emissions (kg N_2O/m^3 WW) were estimated using the following formula:

$$P_{N_2O,on-site} = EF_{N_2O} \cdot \Delta TN \quad (3.4)$$

where EF_{N_2O} is the emission factor (kg N_2O/kg N) with the value of 0.005, related to N_2O production based on influent N loading [36], and ΔTN is the specific difference of TN mass between WWTP influent and effluent (kg N/m^3 WW).

In the off-site CO_2 emissions (kg CO_2/m^3 WW), the following relationship was used, based on [37]:

$$P_{CO_2,off-site} = \frac{(k_{PG} \cdot e_D)}{Q_i} \quad (3.5)$$

where k_{PG} is the emission factor per unit of generated energy to be consumed in the WWTP, its value was taken as 0.323 (kg CO_2 eq./kWh) which is the reported GHG emission intensity of electricity generation for Romania in 2021 [38], e_D (kWh/d) is the energy demand which was calculated as the sum of the aeration and pumping energies (AE+PE), and Q_i is the influent flowrate. The AE and PE indices were computed based on the methods discussed in Chapter 2 [35].

Off-site N_2O emissions were considered due to the biological degradation in the downstream systems of the WWTP, resulting in additional N_2O release. The following equation describes these emissions:

$$P_{N_2O,off-site} = N_e \cdot EF_e \tag{3.6}$$

where N_e is the load of N discharged into the receiving water body, and EF_e is the emission factor of N_2O from the wastewater discharged with a value of $7.857 \cdot 10^{-3}$ (kg N_2O/kg N) [39].

Total GHG emissions was calculated as CO_2 equivalent emissions, based on Eq. (3.7).

$$GHG = P_{CO_2,on-site} + P_{CO_2,off-site} + GWP_{N_2O} \cdot \left(P_{N_2O,on-site} + P_{N_2O,off-site}\right) \tag{3.7}$$

The value for GWP_{N_2O} was taken as 298 [40] to convert emissions in (kg CO_2 eq./m^3 WW) unit.

The optimal values of the gain factors determining the distribution of air in the three aerated bioreactors were searched for by taking into account a 7 days duration scenario. The first two of the three objective functions ($f_{min\ i}$, i=1-3) took into account the energy consumption and GHG emissions of the WWTP as shown in Eqs. (3.10)-(3.11).

$$f_{min,1} = e_D \tag{3.8}$$

$$f_{min,2} = GHG \tag{3.9}$$

For the objective function concerning effluent quality two distinct cases were considered.

In Case 1 the third objective function was considered equal to the ANN predicted EQ:

$$f_{min,3} = EQ \tag{3.10}$$

In Case 2 the EQ was computed based on Eq. (2.4), meaning that 6 distinct GA-NARX models were developed to predict the individual concentrations of the 5 different chemical indicators and the effluent flowrate. The third objective function in Case 2 took into account these individual concentrations and a penalty was applied if the considered limits were not respected (Eq. (3.11)).

$$f_{min,3} = \begin{cases} EQ & if\ COD \leq 125\ \&\ TN \leq 10\ \&\ BOD \leq 25 \\ EQ \cdot \left(1.1 + 0.9 \cdot \frac{t_p}{T}\right) & if\ COD > 125\ or\ TN > 10\ or\ BOD > 25 \end{cases} \tag{3.11}$$

The optimal network hyperparameters and MAPE results for the prediction scenario are shown in Table 3.7.

Table 3.7 GA-NARX model hyperparameters and prediction results

Output	Structure	Architecture	Transfer function(s)	$MAPE_{prediction}$ (%)
AE	open	in-15-out	logsig	1.23
BOD_e	open	in-12-13-out	tansig-tansig	1.14
COD_e	closed	in-11-11-out	tansig-tansig	11.1
EQ	closed	in-13-11-out	tansig-logsig	21.5
GHG	open	in-14-10-out	tansig-logsig	1.24
NO_e	closed	in-14-11-out	tansig-logsig	10.8
PE	open	in-15-15-out	tansig-logsig	4.81
TKN_e	open	in-13-15-out	tansig-tansig	6.27
TSS_e	open	in-15-12-out	logsig-tansig	16.2
Q_e	closed	in-6-13-out	tansig-logsig	0.0457

The optimization result, a Pareto front, from the first optimization case is presented in two 2D graphics instead of a single 3D illustration, shown in Figure 3.4. The location of the three best solutions were also pinpointed with arrows on the graphics.

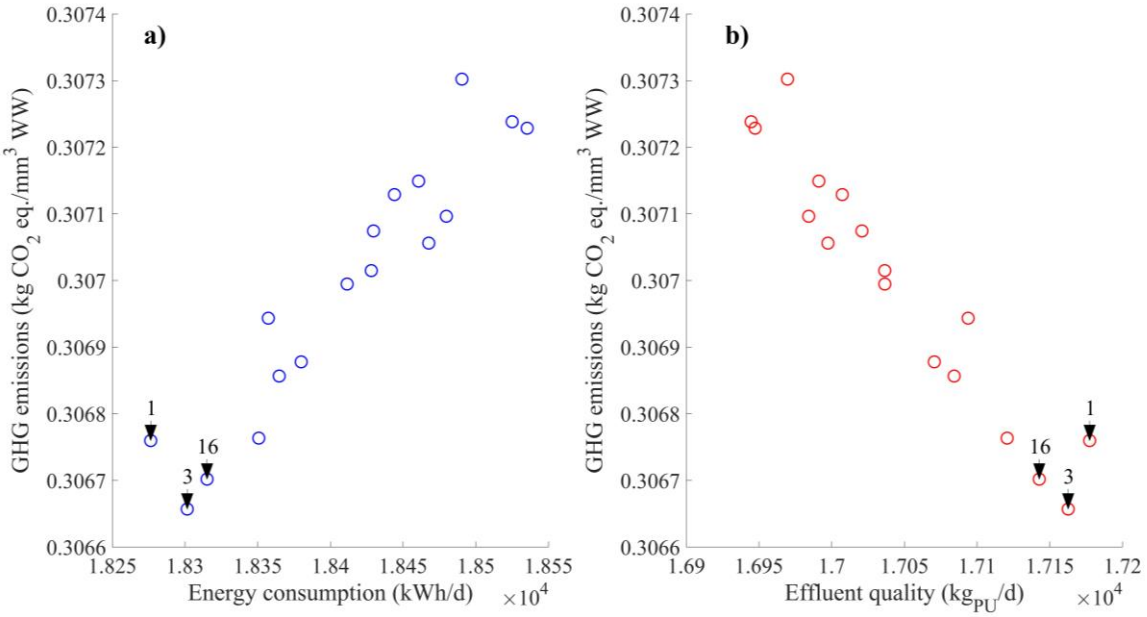

Figure 3.4 Pareto front in Optimization Case 1 shown as: a) GHG emissions *v.s.* energy consumption indices, and b) GHG emissions *v.s.* effluent quality indices

The Pareto front results obtained in Optimization Case 2 are presented in Figure 3.5, similarly to the first optimization case.

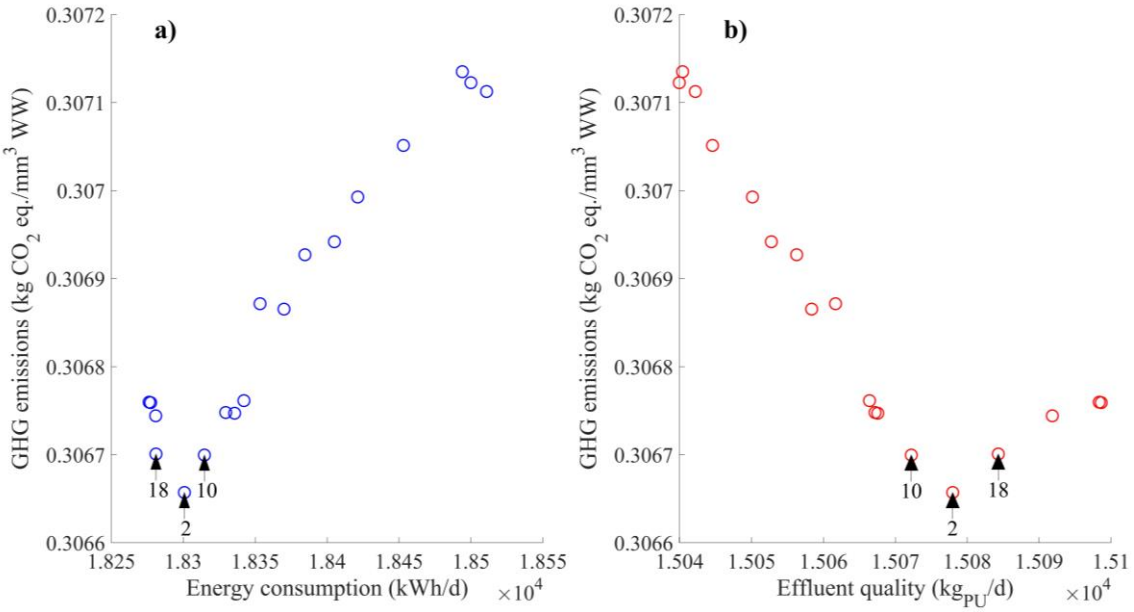

Figure 3.5 Pareto front in Optimization Case 2 shown as: a) GHG emissions v.s. energy consumption indices, and b) GHG emissions v.s. effluent quality indices

The three most promising airflow distribution settings, obtained from both optimization cases, were evaluated by implementing them WWTP first principle extensive model, these results are summarized in Table 3.8.

Table 3.8 WWTP optimized operation performance results

Case	Point number	G1	G2	G3	Energy consumption (kWh/d)	GHG emissions (kg CO_2 eq./m^3 WW)	Effluent quality (kg_{PU}/d)
Base Case		1.000	1.000	1.000	2.025E+04	0.31437	1.479E+04
Optimization Case 1	No. 1	0.8000	0.6000	0.4000	1.984E+04	0.31350	1.465E+04
	No. 3	0.8000	0.6000	0.4304	1.992E+04	0.31366	1.463E+04
	No. 16	0.9092	0.6086	0.4311	1.987E+04	0.31357	1.462E+04
Optimization Case 2	No. 2	0.8000	0.6000	0.4299	1.992E+04	0.31366	1.463E+04
	No. 10	0.8142	0.6001	0.4286	1.991E+04	0.31364	1.463E+04
	No. 18	0.8000	0.6000	0.4105	1.987E+04	0.31355	1.464E+04

The two best optimized cases (Optimization Case 1 number 1 and number 16) were investigated and compared to the Base Case in greater detail, shown in Figure 3.6.

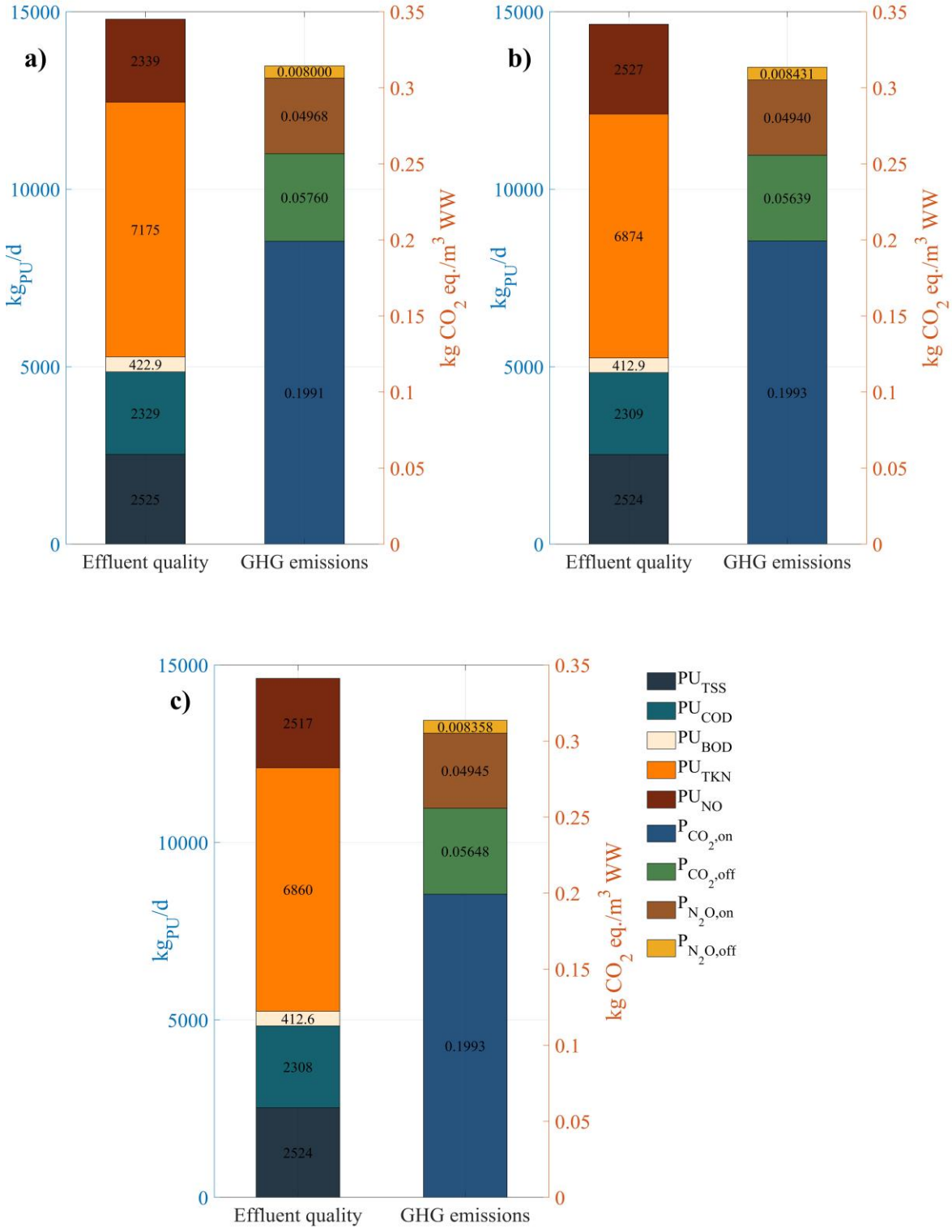

Figure 3.6 Contributions to effluent quality and GHG emissions for: a) Base Case, b) Optimization Case 1 number 1, and c) Optimization Case 1 number 16

3.4. Seasonal DO setpoint optimization for full scale WWTP

In this fourth case study the whole WWTP was assessed, not only the water-line processes but also the sludge ones, when compared to the previous case studies. Moreover, a seasonal modelling approach was adopted as the processes are influenced by the seasonal conditions thus a separate model is required for each period of the year in order to obtain precise models. Similarly to the previous case study, GA were employed in the search of optimal architectures for the ANN models.

The goal of the current study was to address the WWTP seasonal operation optimization taking into account most of the intrinsic biological processes by considering the complex ASM2d and using its dynamic ANN based modelling.

The first novelty of the present work consists in the assessment of effluent quality and plant GHG emissions by ANN models, directly correlating the influent and aeration control related variables to the WWTP performance indices. The second one addresses the optimization based on genetic algorithms of the dynamic artificial neural networks, with the final aim of WWTP seasonal operation optimization. The proposed method for ANN model development consists of employing GA in order to find the optimal NARX hyperparameters, models referred to as GA-NARX. The main steps of the study were:

- Generate, select and pre-process seasonal data for ANN model training.
- Optimize the NARX hyperparameters using GA and find accurate GA-NARX models for the prediction of plant performance indices.
- Use the ANN trained models to optimize with Pareto front the seasonal operation performance of the WWTP by computing the Dissolved Oxygen setpoint of the essential control loop responsible for the aeration.
- Assess performance of the WWTP with optimized setpoints for improving effluent quality and reduce GHG emissions.

Building ANN models substantially relies on the used database and greatly affects the outcome and efficiency of the training process. The current study was performed with simulated data sets, which were obtained by using the Benchmark Simulation Model no. 2 (BSM2), and according to the general characteristics defined in the associated technical report [29]. The utilized model was an extended version of the BSM2 that also describes P, S and Fe transformations, details of which can be found in [41,42]. From the 609 days of BSM2 dynamic inputs, a one-year period was chosen starting from day 45 and encompassing a total of 364 days. The training data were collected from simulations ran with these 364 days, using 15 minutes sample time of the influent dynamics. All of the seasons were considered to be 91 days long, and the 364 days of data was equally split into 4 parts as shown in Figure 3.7.

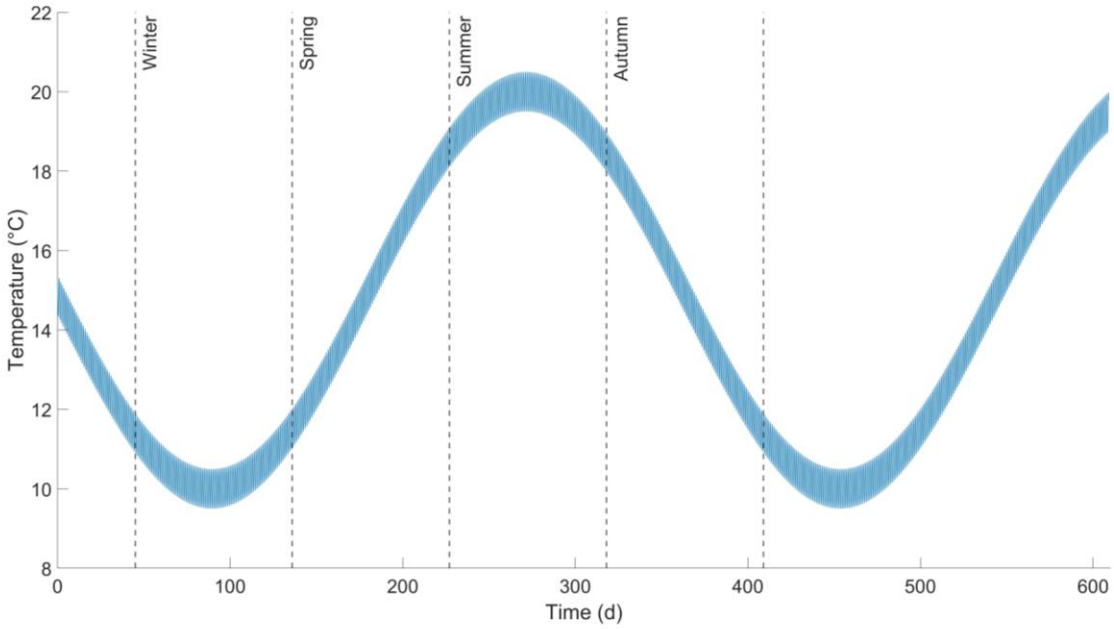

Figure 3.7 Influent temperature changes during the BSM2 609 days dataset and selection of seasonal data

In order to also account for pollution due to P released to the receiving water bodies, an extended version of the EQ criteria was adopted, as described by Eq. (3.12) [42].

$$EQ = \frac{1}{1000 \cdot ts} \cdot \int_{t_i}^{t_{i+1}} \left[PU_{TSS}(t) + PU_{COD}(t) + PU_{BOD_5}(t) + PU_{TKN}(t) + PU_{NO}(t) + PU_{P_{inorg}}(t) + PU_{P_{org}}(t) \right] \cdot Q_e(t) dt \quad (3.12)$$

The effluent quality index assesses the mass of pollutants discharged on a daily basis by considering the effluent values of total suspended solids (PU_{TSS}), chemical oxygen demand (PU_{COD}), biological oxygen demand (PU_{BOD_5}), total Kjeldahl nitrogen (PU_{TKN}), nitrate and nitrite nitrogen (PU_{NO}), inorganic P ($PU_{P_{inorg}}$), organic P ($PU_{P_{org}}$), and by taking into account the effluent flowrate (Q_e). The calculation of EQ and its components was performed as described in [42].

The emissions (kg CO_2 eq./d) released due to the aerobic biological processes, were assessed based on the relationship described in Eq. (3.13) [34].

$$P_{CO_2,ABP} = \left(0.99 \cdot (1 - Y_H) \cdot \eta_{ASP} \cdot bCOD + 1.03 \cdot Y_H \cdot \eta_{ASP} \cdot bCOD \cdot \frac{k_{d,H} \cdot MCRT}{1 + k_{d,H} \cdot MCRT} \right) \cdot Q_i \quad (3.13)$$

here, 0.99 (kg CO2 eq./kg COD) is the emission factor corresponding to organic compounds, Y_H is the heterotrophic biomass yield in (mass VSS/mass COD) with a value of 0.625, η_{ASP} refers to the removal of bCOD in the activated sludge reactors, 1.03 (kg CO_2 eq./kg COD) is an emission factor in relation to the

activated sludge biomass, $k_{d,H}$ is the decay rate for heterotrophic biomass with a value of 0.28 (d^{-1}), *MCRT* is the mean cell residence time, equal to 15 days, and Q_i is the plant influent flowrate (m^3/d).

The CO_2 equivalent (kg CO_2 eq./d) of the N_2O produced in the aerobic biological processes (nitrification and denitrification) was calculated as described by Eq. (3.14), considering a N_2O production equal to 0.5% of the N loading in the influent [36,39].

$$P_{N_2O,ABP} = Q_i \cdot N_{total,i} \cdot 0.005 \cdot GWP_{N_2O} \quad (3.14)$$

The CO_2 production from the use of produced methane was calculated with the assumption that 99% of it is combusted in a gas engine, while the remaining 1% leaks to the atmosphere [36]. The methane production was calculated based on [43], while the produced CO_2 was computed based on the oxidation reaction stoichiometry, as described in Eq. (3.15).

$$P_{CO_2,CH_4} = 0.99 \cdot MP \cdot \frac{44}{16} \quad (3.15)$$

here, *MP* is the mass flowrate of produced methane (kg CH_4/d).

The CO_2 equivalent of the leaked methane was calculated as follows:

$$P_{CH_4} = 0.01 \cdot MP \cdot GWP_{CH_4} \quad (3.16)$$

where GWP_{CH_4} is the global warming potential relative to CO_2 for CH_4, with a value of 28 [19].

The net energy consumption (kWh/d) for the WWTP was calculated as the difference between the daily energy demand and energy recovery. Equations (3.17)-(3.19) present the calculation method for GHG emissions due to energy consumption, energy demand, and energy recovery, respectively.

$$P_{CO_2,energy} = (e_D - e_R) \cdot EF_{energy} \quad (3.17)$$

$$e_D = AE + PE + ME + HE_{net} \quad (3.18)$$

$$e_R = 0.99 \cdot 6 \cdot MP \quad (3.19)$$

here, EF_{energy} is the GHG emission intensity of electricity generation for EU level in the year 2021 with a value of 0.275 kg CO_2 eq./kWh [147], 0.99 is the factor related to the leakage assumption of the produced methane. The calculation of the *AE*, *PE*, *ME*, HE_{net}, *MP* components were performed as described in [43] with a slight difference in the HE_{net} calculation, where the 0.99 factor was also taken into account for the generated heat.

The GHG emission due to sludge disposal to landfills was calculated as the CO_2 (kg CO_2/d) generated from the combustion of biogas in landfills, as shown in Eq. (3.20) [36,44].

$$P_{CO_2,landf} = \frac{110}{113} \cdot W_{S,landf} + \frac{40}{113} \cdot \frac{44}{16} \cdot W_{S,landf} \quad (3.20)$$

where $W_{S,landf}$ is the amount of disposed sludge to landfills (kg VS/d).

The CO_2 equivalent (kg CO_2 eq./d) of the N_2O produced by biological degradation in the downstream system of the WWTP was calculated by Eq. (3.21) [39].

$$P_{N_2O,downs} = \frac{44}{28} \cdot 0.005 \cdot N_{total,e} \cdot GWP_{N_2O} \quad (3.21)$$

here, 44/28·0.005 is the emission factor for N_2O emissions from the treated wastewater (kg N_2O/kg N), and $N_{total,e}$ is the total mass flowrate of N in the effluent (kg N/d).

The best performing GA-NARX models were employed in an optimization task to determine the optimal setpoint value of the DO control loop for the dissolved oxygen in effluent of the second aerated bioreactor considering the core 30-day time period in case of each of the four seasons. The EQ and GHG emissions predictions of the GA-NARX models were used as the two parts of the objective function in a multi-objective optimization task based on GA.

The resulting most favourable solutions emerged from the optimization task of the DO setpoint were tested by dynamic simulation on the mathematical model. For a thorough evaluation of the optimized WWTP operation, the operational cost index (OCI) was also calculated for both the optimized and base case. The OCI describes the operation of the wastewater treatment process by relating it to cost factors. It is calculated as a weighted sum of the costs in the WWTP and is described in Eq. (3.23).

$$OCI = 3 \cdot SP + 3 \cdot EC + e_D - e_R \tag{3.23}$$

The metrics taken into consideration when selecting the most accurate ANN model for further use were the MSE, MAPE, and R^2. Two separate scenarios were investigated considering the definition of the most accurate model. In the first case (Case 1), the model was saved if all three of the evaluation metrics outperformed the previously obtained best results. In the second case (Case 2), the network was saved when any of the three metrics presented better results than the previous top result of that metric.

The most performant networks modelling EQ displayed R^2 values ranging from 0.9930 to 0.9950. While in the case of MAPE values, these were situated between 3.53% and 4.25%. Regarding the GA-NARX modelling GHG emissions, the resulted ranges for these values were 0.9867 to 0.9872 and 2.79% to 2.88% for R^2 and MAPE, respectively. The accuracy of the developed ANN models was found similar to values reported in literature.

The optimal DO settings selected for testing on the 30-day periods from each seasonal dataset are associated to the points highlighted with a red circle in Figure 3.8. The values obtained from the Pareto fronts that were tested by dynamic simulation on the mathematical model were: 1.373 mg O_2/L for the winter, 1.911 mg O_2/L for spring, 1.553 mg O_2/L for summer, and 1.837 mg O_2/L for the autumn season. Each of the aforementioned values were applied as setpoints to the DO controller for the core 30-day test period of each season. The EQ, GHG emissions, and OCI obtained by implementing these setpoints were compared to the results of the base case. These results are presented in Table 3.9. The relative differences (Relative diff.) between the base and optimized cases were also calculated to better display the amount of change and incentives that the optimized case brought relative to the base case.

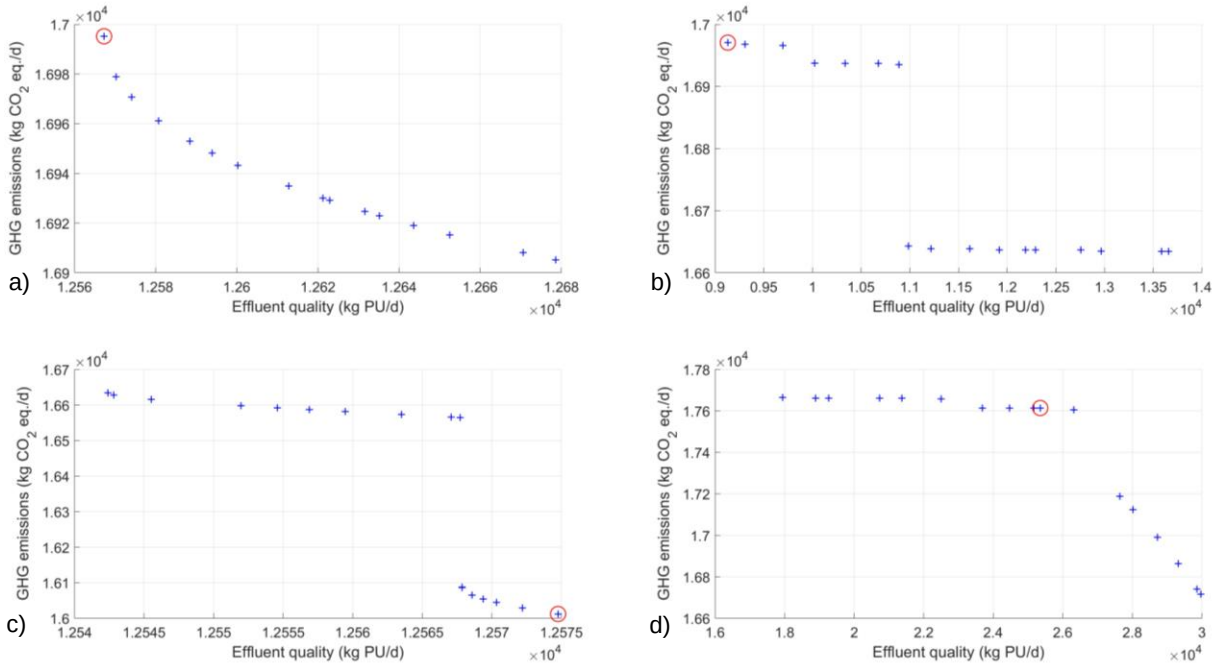

Figure 3.8 Pareto fronts and selected solutions for testing on seasonal data from: a) winter, b) spring, c) summer, and d) autumn

The OCI values for the optimized cases presented improvements for all seasonal data with values ranging between 0.25% and 0.90%. Similar to GHG, this index is also influenced through the change in energy consumption brought by the lower DO setpoint values. As a result of operation optimization, the simultaneous decrease in both EQ and OCI was achieved for all seasonal data, signifying that a more performant treatment process was achieved in terms of kg PU per OCI units. Overall, the results indicated that the different seasonal scenarios require distinct settings to achieve an improved WWTP operation.

It is also important to note that the computer processing time and computation resources for the multi-objective optimization task was greatly reduced due to the use of GA-NARX models. The time necessary to finish the multi-objective optimization procedure by reaching the considered fixed generations limit was around 600 seconds. Concurrently, a single simulation of the 30-day time period using the first principle mathematical model took more than 630 seconds, using the same computational power. Assuming that the same optimization employing the first principle mathematical model for objective function computation would need the same number of iterations to finish, it would obtain results in four orders of magnitude higher processing time. In other words, the search of the optimal setting for a 30-day scenario would require close to 73 days of computation when the first principle model is used, while the same optimization task is performed by the developed GA-NARX models in 10 minutes.

Table 3.9 EQ, GHG, and OCI results obtained from the base and optimized cases

	Winter			Spring			Summer			Autumn		
Case	EQ	GHG	OCI	EQ	GHG	OCI	EQ	GHG	OCI	EQ	GHG	OCI
	kg PU/d	kg CO_2 eq./d	-	kg PU/d	kg CO_2 eq./d	-	kg PU/d	kg CO_2 eq./d	-	kg PU/d	kg CO_2 eq./d	-
Base case	13158	16819	9256	12555	16584	9544	13034	16713	10384	12961	16950	10275
Optimized	12252	16804	9226	12355	16571	9518	11299	16646	10290	12375	16926	10249
Relative diff. (%)	-6.88	-0.09	-0.33	-1.60	-0.08	-0.26	-13.31	-0.40	-0.90	-4.52	-0.14	-0.25

4. Detection and identification of DO sensor fault types via ANN models

AI techniques have been aimed to perform sensor fault detection and error type diagnosis in a variety of fields. They were proven to be an effective tool, intended to target various implementations in WWTPs for. One fault diagnosis using ANNs was successfully applied to sludge bulking measurements with the intention of ensuring process safety and WWTP effluent quality. The developed model could differentiate five types of sludge bulking faults [45]. However, artificial neural networks were scarcely applied to the identification of the WWTP sensor faults, but their potential is significant.

The scope of the current study was to design, train and test the performance of an ANN based tool that is capable of detection and identification of seven types of Dissolved Oxygen sensor faults. The novelty consists in the application of proposed ANN diagnosis tool for the municipal A^2O configuration WWTP, having implemented the two main control loops, one for nitrification and another for denitrification (Figure 3.2).

The data implied by the development of the ANN fault identification tool were obtained using a previously calibrated first-principle Activated Sludge Model no.1 of the WWTP considered as case study. Seven types of sensor faults were simulated for the Dissolved Oxygen sensor: bias, also known as shift or off-set of the signal; complete failure, which can be maximum or minimum and occurs when the measured value is either the highest or the lowest value of the sensor calibration range; drift, which is an irregularly varying deviation in time of the measured value, compared to the true DO one; fixed value, when the DO signal value is constant; loss of accuracy, meaning that the value provided by the sensor is affected by imprecision around the true value; wrong gain, known also as a typical calibration error [46].

The dataset was divided in the following parts when the Levenberg-Marquardt training algorithm was employed: 70% for training, 15% for validation, and 15% for testing. The training results showed good results, with the exception of the highest obtained confusion value of 58.7%, due to the confusion between the complete failure maximum (class 3) and fixed value (class 6) fault types, characterized by comparable effects.

In comparison to the first training approach, the classification performed by the second trained ANN that used the Bayesian regularization algorithm showed better results. Results obtained for the testing data set are presented in Figure 4.1. This method of training did not require a validation dataset. Consequently, 85% of the data were used for training, while the remaining 15% constituted the testing dataset. In terms of training, the highest confusion value was of 1.1% in case of the wrong gain fault, where out of 1920 data points only 21 were classified as other fault classes.

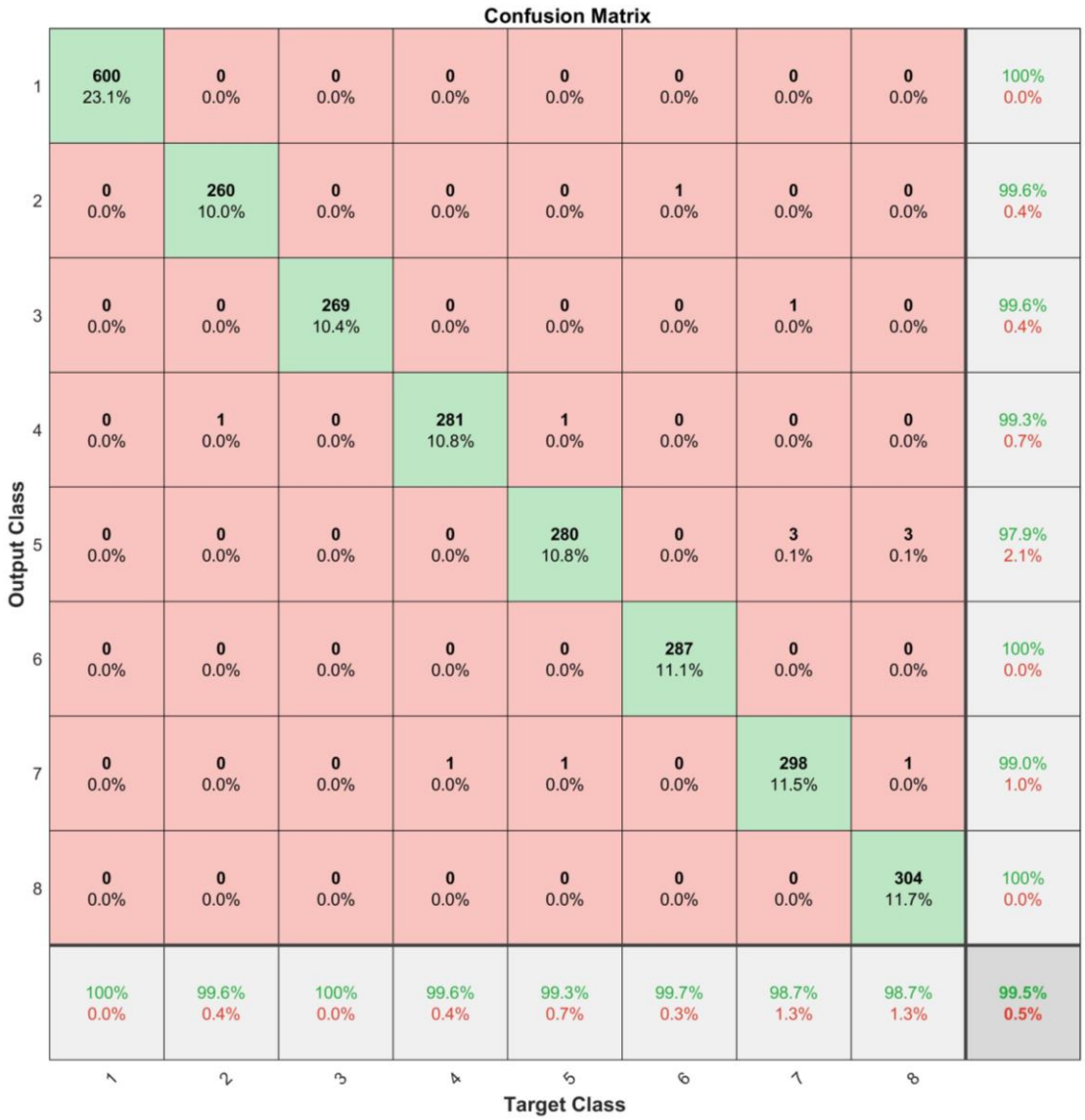

Figure 4.1 Confusion matrix of the testing dataset for ANN trained with Bayesian regularization algorithm

The correct identification of the fault type may take different time periods, depending on the fault type. Predominantly, the classification network quickly and correctly identified the different fault types. These time periods of the firmly correct identification are: 3 hours for bias, 2.5 hours in case of complete fail maximum, 2.5 hours at complete fail minimum, 3 hours for drift, 3.5 hours for fixed, 4 hours at loss of accuracy, and the longest identification of 11 hours in case of wrong gain also shown in Figure 4.2.

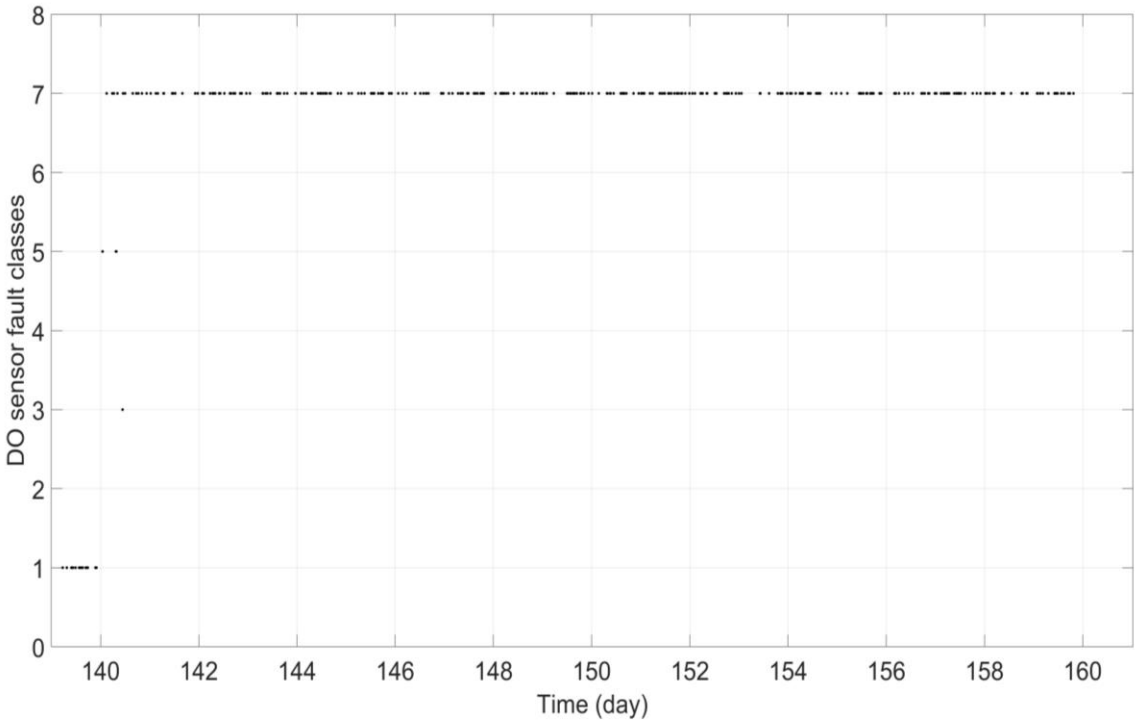

Figure 4.2 Classification of the testing dataset for loss of accuracy type of DO sensor fault

5. Concluding remarks

The research performed in the current thesis focused on improving the operation of the wastewater treatment plant. A key aspect of the studies was the development of accurate ANN models in order for these to be utilized in either optimization (Chapter 3) or fault detection and identification tasks (Chapter 4). The wastewater treatment process was evaluated in terms of GHG emissions, energy consumption, effluent quality, and overall cost.

Section 3.1 focused on the optimization of recycle flowrates that influence the biological nutrient removal processes in a setting when the system does not have control loops. First of all, a previously developed Matlab/Simulink model calibrated on real plant data was employed to generate the dataset for the development of four types of ANN models. These were designed to directly output the WWTP evaluation criteria without further need for calculations. The input features of these models consisted of the influent and plant operation parameters. A full factorial design was employed to find the best network architectures for both MISO and MIMO models. The models were validated on a separate dataset which was not utilized in their training and their performance was compared to models found in the literature. This development process resulted in ANN models that showed nearly optimal values in terms of R^2 values and highly satisfactory MAPE values, which ranged from 0.89 to 0.99 and 0.85 to 3.50, respectively.

This was followed by the implementation of the best ANN models in the optimization task where two gain factors were searched for that influence the flow rates of the internal and external recycle streams taking into account a 7-day scenario. In this case study the weighted sum of the aeration energy, pumping energy, and effluent quality represented the objective function. The results were tested on the Simulink model and compared to the reference case and the optimization when the mathematical model was used. The optimal values found by the ANNs showed that energy consumption could be reduced by 4.2% although the effluent quality slightly worsened. The values found using the mathematical model itself could be considered superior as the energy demand was reduced by nearly the same amount accompanied by a marginal improvement in effluent quality. However, the optimization process with the ANN models was four orders of magnitude shorter, demonstrating promising potential in real-time applications.

Section 3.2 presents the optimization of control loop setpoints concerning the two control loops acting on the flowrates of the internal and external recycle streams. A similar approach was adopted in terms of data generation and ANN model development, i.e., four types of ANNs were considered that modelled the energy and effluent quality indices based on influent and plant operation parameters, in case of both MISO and MIMO structures. In addition, this study investigated the influence of the input delay on the accuracy of developed neural networks. This hyperparameter is essential in dynamic modeling and was seldom discussed in the literature, especially in WWTP modelling applications. The optimization of this

hyperparameter led to improvements in the networks' accuracy from a range of 1.51 to 3.09 to a range of 1.27 to 2.57 in terms of MAPE values, and from values between 0.95 and 1.00 to values between 0.97 to 1.00 when looking at R^2 results.

These improved ANN models were employed in the optimization of the two control loops for a week-long scenario. The objective function was once more defined as a weighted sum of the three WWTP performance indices. The optimization task was also performed by the use of the mathematical model, and the results were put into comparison with the ones obtained by the ANN models and a reference case. The solutions found by the ANN structures and the first-principle model were very similar. However, this time the neural networks outperformed the classic approach with improvements of 8.9% and 2% with respect to energy consumption and effluent quality, while they were also faster by around 200 times.

Section 3.3 discusses the optimization of a novel strategy pertaining to the distribution of air flowrate in the aerated bioreactor. The uneven distribution of compressed air is proposed in order to facilitate the rate of the biological processes at the beginning of the aerated bioreactor. In this study, the WWTP operation was evaluated in terms of energy efficiency, effluent quality, as well as GHG emissions. MISO structures were taken into account for the two types of NARX that were considered, but the development of ANN models also included a novel approach, i.e., an optimization task performed by GA for the purpose of finding the most appropriate architectures to model not only the performance indices, but various effluent concentrations as well as the WWTP's emissions. The use of neural networks to model the GHG emissions was yet to be investigated in this field of study. The emissions took into account both on-site and off-site emissions for CO_2 and N_2O gases. The accuracy of obtained GA-NARX models varied from 0.05 to 21.5 MAPE values, when presented with a new set of input data.

The best GA-NARX models were utilized in two multi-objective optimization tasks of a 7-day scenario, searching for the best aeration gain factors when the objective functions of the multi-objective optimization were the energy consumption, effluent quality, and energy consumption. The first optimization case employed the models for the performance indices and GHG emissions, whereas the second optimization case used the models for effluent concentrations, energy indices, and GHG emissions. At the same time, the second optimization case took into account the local regulations for pollutant concentrations in the effluent and penalties were issued for solutions that did not respect these. The two optimization tasks resulted in a Pareto front each, both containing 18 possible scenarios for the three aeration gain factors. These were ranked, and the best three from each front were tested on the mathematical model and compared to the reference scenario. Energy demand and GHG emission were both reduced by up to 2%, while effluent quality was also improved by up to 1.1%. Investigation of the EQ and GHG contributions of the different sources revealed that the improvement of EQ can be attributed mostly to the lowering of TKN levels, while

the reduction in GHG emission can be assigned to the off-site CO_2 emissions due to a decrease in energy consumption, validating the proposed operation strategy.

Section 3.4 focused on a recently introduced notion of seasonal modelling of the WWTP and coupled it with multi-objective optimization of the dissolved oxygen control loop setpoint for a full-scale WWTP. The study presented in this section utilized an extended version of the BSM2 for data generation, while the previously discussed GA-NARX methodology was applied for ANN model development, however the optimized hyperparameters were extended with the training algorithm for which the three most commonly employed in this field of study were considered. The networks had 13 input features consisting of influent and operation parameters and predicted the effluent quality and GHG emissions of the WWTP. In this case, CH_4 emissions were also taken into consideration. The ANN model testing results showed a performance range of 0.987 to 0.995 in terms of R^2, while the values for MAPE situated between 2.79 and 4.25.

The optimal DO setting was searched for a 30-day time period taking into account effluent quality and GHG emissions as the two objectives for the multi-objective optimization task. The optimization was performed for all four seasons offering a set of 18 possible solutions for each season, known as a Pareto front. The solution considered as best was tested on the mathematical model and compared to the reference case. The DO values for the seasons ranged from 1.373 to 1.911 mg O_2/L, the implementation of these improved effluent quality by up to 13.3% and also slightly reduced GHG emissions by less than 1%. These enhancements of the WWTP operation were also accompanied by reduction of the overall cost by almost 1%. The reduction in emissions were attributed to the reduction in energy consumption which is due to the lower DO setpoints than the reference value. The optimization task utilizing the GA-NARX models finished in a matter of minutes, while the same task would have taken more than 30 days for the 30-day scenario, i.e., a four orders of magnitude difference. The neural network models showcased their promising potential for various application purposes such as support for decision-making or model-based control of WWTP operation.

Chapter 4 presents the investigation of ANN models as soft tools for detection and identification of DO sensor faults. Similar soft tools were investigated in the literature, however were yet to be applied in case of wastewater treatment plants. Seven fault types were considered in the study, and the calibrated Matlab/Simulink model was utilized for data generation purposes. The networks were developed using 20 input features encompassing influent variables and concentration of several species from the secondary clarifier's bottom effluent, while the objective of the network was to classify the operation of the sensor into one of 8 categories, i.e., normal functioning and the seven fault types. A trial-and-error process was employed to find for the best performing neural network model by searching for optimal the architecture and training algorithm. The considered training methods were the Levenberg-Marquardt and Bayesian regularization algorithms.

The most accurate network developed with each training algorithm was tested with a new set of input data. Both ANN models had outstanding performances looking at the detection of fault types, the network trained with Levenberg-Marquardt algorithm showed a confusion percentage of 0%, indicating that the classification was correct in 100% of the cases, similarly, the network trained with Bayesian regularization also performed impeccably with 0% confusion. The differences between the networks were revealed at the identification of fault types, where the ANN trained with Levenberg-Marquardt algorithm gravely confused two types of errors with each resulting in confusion rates of 44.2% and 41.3% for the two, while it had an overall accuracy of 85.7%. On the other hand, the neural network trained with Bayesian regularization demonstrated a much higher degree of accuracy, with the largest confusion value of 1.3% for an individual class and an almost ideal overall accuracy of 99.5%. At the same time, the correct identification of the fault types was performed in a matter of hours since the beginning of the faulty behaviour. The developed ANN shows promise in utilization for the precise monitoring of processes at the WWTP, supporting their safe and effective operation.

Future work may focus on connecting together aspects of the several studies for an overall optimization of the WWTP operation or on broadening the present investigations to include other types of data-driven models as well as other operation strategies.

References

[1] Le Treut H., R. Somerville, U. Cubasch, Y. Ding, C. Mauritzen, A. Mokssit, T. Peterson and M. Prather, 2007: Historical Overview of Climate Change. In: Climate Change 2007: The Physical Science Basis. Contribution of Working Group I to the Fourth Assessment Report of the Intergovernmental Panel on Climate Change [Solomon, S., D. Qin, M. Manning, Z. Chen, M. Marquis, K.B. Averyt, M. Tignor and H.L. Miller (eds.)]. Cambridge University Press, Cambridge, United Kingdom and New York, NY, USA.

[2] Calvin K, Dasgupta D, Krinner G, Mukherji A, Thorne PW, Trisos C, et al. IPCC, 2023: Climate Change 2023: Synthesis Report. Contribution of Working Groups I, II and III to the Sixth Assessment Report of the Intergovernmental Panel on Climate Change [Core Writing Team, H. Lee and J. Romero (eds.)]. IPCC, Geneva, Switzerland. 2023. https://doi.org/10.59327/IPCC/AR6-9789291691647.

[3] International Energy Agency (IEA). Tracking power 2020. Paris: 2020.

[4] IEA. Coal-Fired Power. Paris: 2020.

[5] Gu Y, Li Y, Yuan F, Yang Q. Optimization and control strategies of aeration in WWTPs: A review. J Clean Prod 2023:138008. https://doi.org/10.1016/j.jclepro.2023.138008.

[6] Aghabalaei V, Nayeb H, Mardani S, Tabeshnia M, Baghdadi M. Minimizing greenhouse gases emissions and energy consumption from wastewater treatment plants via rational design and engineering strategies: A case study in Mashhad, Iran. Energy Reports 2023;9:2310–20. https://doi.org/10.1016/j.egyr.2023.01.017.

[7] Zhao Y, Wesley Awe O, Liu R. Analysis of Energy Consumption and Saving in Wastewater Treatment Plant : Case Study from Ireland Analysis of Energy Consumption and Saving in Wastewater Treatment Plant: Case Study from Ireland. J Water Sustain 2016;2:63–76. https://doi.org/10.11912/jws.2016.6.2.63-76.

[8] Cardoso BJ, Rodrigues E, Gaspar AR, Gomes Á. Energy performance factors in wastewater treatment plants: A review. J Clean Prod 2021;322:129107. https://doi.org/10.1016/j.jclepro.2021.129107.

[9] Qadir M, Drechsel P, Jiménez Cisneros B, Kim Y, Pramanik A, Mehta P, et al. Global and regional potential of wastewater as a water, nutrient and energy source. Nat Resour Forum 2020;44:40–51. https://doi.org/10.1111/1477-8947.12187.

[10] Di Fraia S, Massarotti N, Vanoli L. A novel energy assessment of urban wastewater treatment plants. Energy Convers Manag 2018;163:304–13. https://doi.org/10.1016/j.enconman.2018.02.058.

[11] Our World in Data. Electricity production by source. https://ourworldindata.org/grapher/electricity-prod-source-stacked?stackMode=relative (accessed September 14, 2023).

[12] Ranieri E, D'Onghia G, Lopopolo L, Gikas P, Ranieri F, Gika E, et al. Evaluation of greenhouse gas emissions from aerobic and anaerobic wastewater treatment plants in Southeast of Italy. J Environ Manage 2023;337:117767. https://doi.org/10.1016/j.jenvman.2023.117767.

[13] Henze M, Gujer W, Mino T, van Loosedrecht M. Activated Sludge Models ASM1, ASM2, ASM2d and ASM3. Water Intell Online 2015;5:9781780402369–9781780402369. https://doi.org/10.2166/9781780402369.

[14] Simon Haykin. Neural Networks and Learning Machines. Third Edition. McMaster University, Canada: Pearson; 2008.

[15] Zounemat-Kermani M, Stephan D, Hinkelmann R. Multivariate NARX neural network in prediction gaseous emissions within the influent chamber of wastewater treatment plants. Atmos Pollut Res 2019;10:1812–22. https://doi.org/10.1016/j.apr.2019.07.013.

[16] Zhu L, Wang C, Huang N, Fu Y, Yan Z. Developing an Indicator System to Monitor City's Sustainability Integrated Local Governance: A Case Study in Zhangjiakou. Sustainability 2022;14:5047. https://doi.org/10.3390/su14095047.

[17] Du W-J, Lu J-Y, Hu Y-R, Xiao J, Yang C, Wu J, et al. Spatiotemporal pattern of greenhouse gas emissions in China's wastewater sector and pathways towards carbon neutrality. Nat Water 2023;1:166–75. https://doi.org/10.1038/s44221-022-00021-0.

[18] Wang D, Ye W, Wu G, Li R, Guan Y, Zhang W, et al. Greenhouse gas emissions from municipal wastewater treatment facilities in China from 2006 to 2019. Sci Data 2022;9:317. https://doi.org/10.1038/s41597-022-01439-7.

[19] IPCC, 2014: IPCC Fifth Assessment Report: Climate Change 2014 (AR5). https://www.ipcc.ch/report/ar5/syr/ (accessed September 12, 2023).

[20] Bani Shahabadi M, Yerushalmi L, Haghighat F. Estimation of greenhouse gas generation in wastewater treatment plants - Model development and application. Chemosphere 2010;78:1085–92. https://doi.org/10.1016/j.chemosphere.2009.12.044.

[21] Daelman MRJ, van Voorthuizen EM, van Dongen LGJM, Volcke EIP, van Loosdrecht MCM. Methane and nitrous oxide emissions from municipal wastewater treatment – results from a long-term study. Water Sci Technol 2013;67:2350–5. https://doi.org/10.2166/wst.2013.109.

[22] Åmand L, Olsson G, Carlsson B. Aeration control – a review. Water Sci Technol 2013;67:2374–98. https://doi.org/10.2166/wst.2013.139.

[23] Ba-Alawi AH, Al-masni MA, Yoo C. Simultaneous sensor fault diagnosis and reconstruction for intelligent monitoring in wastewater treatment plants: An explainable deep multi-task learning model. J Water Process Eng 2023;55:104119. https://doi.org/10.1016/j.jwpe.2023.104119.

[24] Ba-Alawi AH, Loy-Benitez J, Kim S, Yoo C. Missing data imputation and sensor self-validation towards a sustainable operation of wastewater treatment plants via deep variational residual autoencoders. Chemosphere 2022;288:132647. https://doi.org/10.1016/j.chemosphere.2021.132647.

[25] Ge Z, Song Z, Gao F. Review of Recent Research on Data-Based Process Monitoring. Ind Eng Chem Res 2013;52:3543–62. https://doi.org/10.1021/ie302069q.

[26] Xi J, Gong H, Zhang Y, Dai X, Chen L. The evaluation of GHG emissions from Shanghai municipal wastewater treatment plants based on IPCC and operational data integrated methods (ODIM). Sci Total Environ 2021;797:148967. https://doi.org/10.1016/j.scitotenv.2021.148967.

[27] Várhelyi M, Cristea VM, Brehar M, Nemeș ED, Nair A. WWTP model calibration based on different optimization approaches. Environ Eng Manag J 2019;18:1657–70. https://doi.org/10.30638/eemj.2019.156.

[28] Otterpohl R. Dynamische Simulation zur Unterstützung der Planung und des Betriebes von kommunalen Kläranlagen. PhD thesis 1995.

[29] Alex J, Benedetti L, Copp J, Gernaey K V., Jeppsson U, Nopens I, et al. Benchmark Simulation Model no . 2 (BSM2). Iwa 2018;1:99.

[30] Gan M, Peng H, Dong XP. A hybrid algorithm to optimize RBF network architecture and parameters for nonlinear time series prediction. Appl Math Model 2012;36:2911–9. https://doi.org/10.1016/j.apm.2011.09.066.

[31] Simon-Várhelyi M, Cristea VM, Luca AV. Reducing energy costs of the wastewater treatment plant by improved scheduling of the periodic influent load. J Environ Manage 2020;262. https://doi.org/10.1016/j.jenvman.2020.110294.

[32] Ostace G.S., V.M. Cristea, P.S. Agachi, Extension of Activated Sludge Model No 1 with Two-Step Nitrification and Denitrification Processes for Operation Improvement, Environ Eng Manag J. 10 2011 1529–1544. https://doi.org/10.30638/eemj.2011.214..

[33] Ojha VK, Abraham A, Snášel V. Metaheuristic design of feedforward neural networks: A review of two decades of research. Eng Appl Artif Intell 2017;60:97–116. https://doi.org/10.1016/j.engappai.2017.01.013.

[34] Gori R, Jiang LM, Sobhani R, Rosso D. Effects of soluble and particulate substrate on the carbon and energy footprint of wastewater treatment processes. Water Res 2011;45:5858–72. https://doi.org/10.1016/j.watres.2011.08.036.

[35] Alex J, Benedetti L, Copp J, Gernaey K V, Jeppsson U, Nopens I, et al. Benchmark Simulation Model no . 1 (BSM1). vol. 1. 2008.

[36] Koutsou OP, Gatidou G, Stasinakis AS. Domestic wastewater management in Greece: Greenhouse gas emissions estimation at country scale. J Clean Prod 2018;188:851–9. https://doi.org/10.1016/j.jclepro.2018.04.039.

[37] Mannina G, Ekama G, Caniani D, Cosenza A, Esposito G, Gori R, et al. Greenhouse gases from wastewater treatment - A review of modelling tools. Sci Total Environ 2016;551–552:254–70. https://doi.org/10.1016/j.scitotenv.2016.01.163.

[38] EEA, 2022: Data visualization: Country level – Greenhouse gas emission intensity of electricity generation. https://www.eea.europa.eu/data-and-maps/daviz/co2-emission-intensity-12/#tab-chart_2 (accessed September 14, 2023).

[39] IPCC, 2006: IPCC Guidelines for National Greenhouse Gas Inventories. https://www.ipcc-nggip.iges.or.jp/public/2006gl/vol5.html (accessed September 14, 2023).

[40] IPCC, 2007: Climate Change 2007: Synthesis Report. Contribution of Working Groups I, II and III to the Fourth Assessment Report of the Intergovernmental Panel on Climate Change [Core Writing Team, Pachauri, R.K and Reisinger, A. (eds.)]. IPCC, Geneva, Switzerland.

[41] Flores-Alsina X, Solon K, Kazadi Mbamba C, Tait S, Gernaey K V., Jeppsson U, et al. Modelling phosphorus (P), sulfur (S) and iron (Fe) interactions for dynamic simulations of anaerobic digestion processes. Water Res 2016;95:370–82. https://doi.org/10.1016/j.watres.2016.03.012.

[42] Solon K, Flores-Alsina X, Kazadi Mbamba C, Ikumi D, Volcke EIP, Vaneeckhaute C, et al. Plant-wide modelling of phosphorus transformations in wastewater treatment systems: Impacts of control and operational strategies. Water Res 2017;113:97–110. https://doi.org/10.1016/j.watres.2017.02.007.

[43] Gernaey K V., Jeppsson U (Ulf), Vanrolleghem PA, Copp JB, International Water Association. Task Group on Benchmarking of Control Strategies for Wastewater Treatment Plants. Benchmarking of

control strategies for wastewater treatment plants. 2014.

[44] Mamais D, Noutsopoulos C, Dimopoulou A, Stasinakis A, Lekkas TD. Wastewater treatment process impact on energy savings and greenhouse gas emissions. Water Sci Technol 2015;71:303–8. https://doi.org/10.2166/wst.2014.521.

[45] Han H-G, Liu H-X, Liu Z, Qiao J-F. Fault detection of sludge bulking using a self-organizing type-2 fuzzy-neural-network. Control Eng Pract 2019;90:27–37. https://doi.org/10.1016/j.conengprac.2019.06.010.

[46] Luca AV, Simon-Várhelyi M, Mihály NB, Cristea VM. Data driven detection of different dissolved oxygen sensor faults for improving operation of the wwtp control system. Processes 2021;9. https://doi.org/10.3390/pr9091633.